

# CONTROLLABLE INVERSION OF BLACK-BOX FACE-RECOGNITION MODELS VIA DIFFUSION

PREPRINT. UNDER REVIEW.

<b>Manuel Kansy*</b> ETH Zurich manuel.kansy@inf.ethz.ch	<b>Anton Raël</b> ETH Zurich anrael@student.ethz.ch	<b>Graziana Mignone</b> DisneyResearch Studios graziana.mignone@disneyresearch.com
<b>Jacek Naruniec</b> DisneyResearch Studios jacek.naruniec@disneyresearch.com	<b>Christopher Schroers</b> DisneyResearch Studios christopher.schroers@disneyresearch.com	
<b>Markus Gross</b> ETH Zurich grossm@inf.ethz.ch	<b>Romann M. Weber</b> DisneyResearch Studios romann.weber@disneyresearch.com	

March 23, 2023

## ABSTRACT

Face recognition models embed a face image into a low-dimensional identity vector containing abstract encodings of identity-specific facial features that allow individuals to be distinguished from one another. We tackle the challenging task of inverting the latent space of pre-trained face recognition models without full model access (*i.e. black-box* setting). A variety of methods have been proposed in literature for this task, but they have serious shortcomings such as a lack of realistic outputs, long inference times, and strong requirements for the data set and accessibility of the face recognition model. Through an analysis of the black-box inversion problem, we show that the conditional diffusion model loss naturally emerges and that we can effectively sample from the inverse distribution even without an identity-specific loss. Our method, named identity denoising diffusion probabilistic model (ID3PM), leverages the stochastic nature of the denoising diffusion process to produce high-quality, identity-preserving face images with various backgrounds, lighting, poses, and expressions. We demonstrate state-of-the-art performance in terms of identity preservation and diversity both qualitatively and quantitatively. Our method is the first black-box face recognition model inversion method that offers intuitive control over the generation process and does not suffer from any of the common shortcomings from competing methods.

**Keywords** Black-box inversion · face recognition models · diffusion models · image generation · controllable face generation

## 1 Introduction

Face recognition systems are omnipresent nowadays. Their applications range from classical use cases such as access control of smartphones to newer ones such as tagging a picture by identity or even controlling the output of generative models [25, 2, 42]. The goal of a face recognition method  $f$  is to obtain embeddings  $y$  of face images  $x$  such that the embeddings of images of the same person are closer to each other than those of images of other people. We refer to this embedding  $y$  as the *identity vector* or *ID vector*. In this paper, we propose a technique to sample from  $p(x|y)$ , *i.e.* to produce realistic face images from an ID vector.

---

\*Corresponding author.

By design, the many-to-one mapping of face recognition methods assigns multiple images of a given identity to the same identity representation. The inverse one-to-many problem, *i.e.* producing a high-dimensional image from a low-dimensional ID vector, is extremely challenging. Previous methods often rely on the gradient of face recognition models either directly [71] or use it during training in the form of a loss function [4, 42]. This gradient or information about the model’s architecture and weights is often not available, *e.g.* if using an API of a proprietary model. We therefore focus on the more generally applicable *black-box* setting, where only the resulting ID vectors are available. In addition to being more general, the black-box setting has the additional benefit that we can easily extend our conditioning mechanism to include information from different, even non-differentiable sources (*e.g.* labels, biological signals).

We propose the intity denoising diffusion probabilistic model (ID3PM), the first method that uses a diffusion model to invert the latent space of a face recognition model, *i.e.* to generate highly realistic, identity-preserving face images conditioned solely on black-box ID vectors as seen in Fig. 1. We show mathematically that we can effectively invert a model  $f$  even without having access to its gradients by using a conditional diffusion model. This allows us to train our method with an easy-to-obtain data set of pairs of images and corresponding ID vectors without an identity-specific loss term.

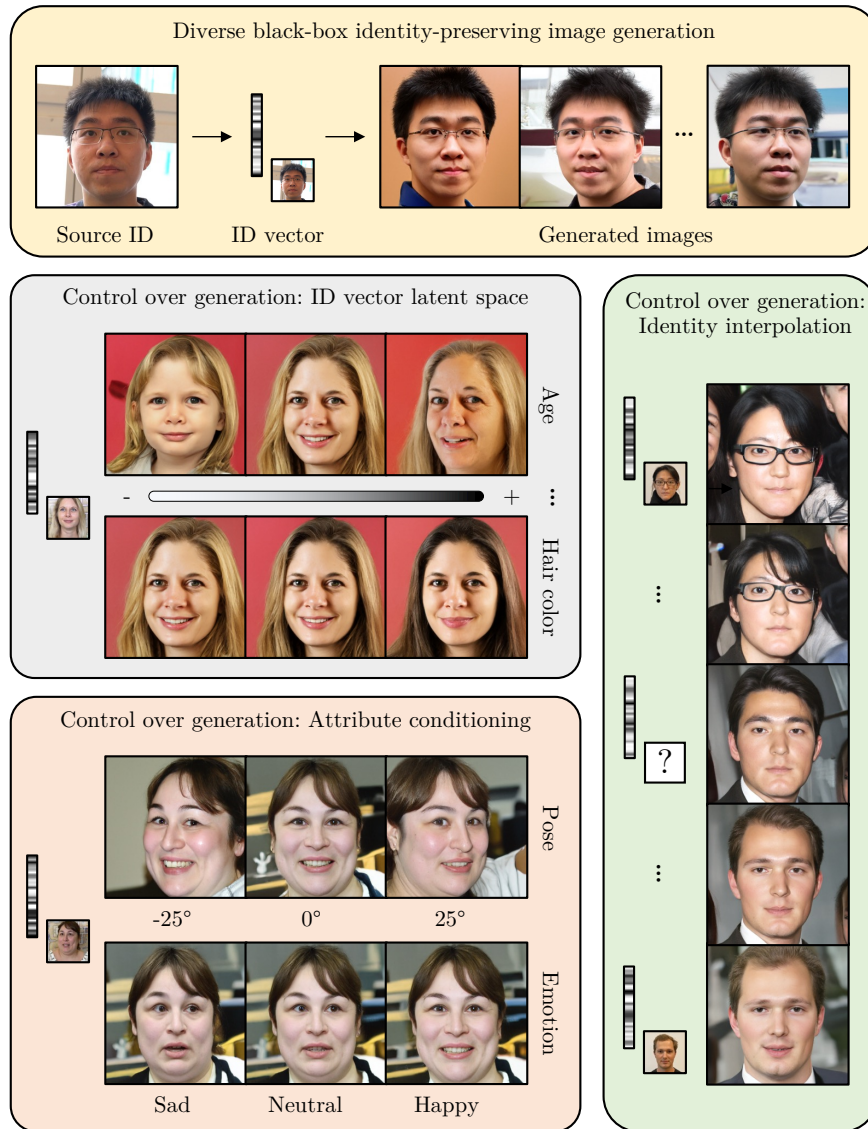


Figure 1: Overview. Our method inverts a pre-trained face recognition model (here InsightFace [8]) to produce high-quality identity-preserving images. We are the first black-box method to provide intuitive control over the image generation process.



Our method demonstrates state-of-the-art performance for the inversion task and also allows for controllability over the generation process as seen in Fig. 1. To the best of our knowledge, our method is the first black-box face recognition model inversion method to do so. Specifically, we can control (1) the diversity among samples generated from the same ID vector via the classifier-free guidance scale, (2) identity-specific features (*e.g.* age) via smooth transitions in the ID vector latent space, which also enables identity interpolations, and (3) identity-agnostic features (*e.g.* pose) via explicit attribute conditioning.

To summarize, our main contributions are:

1. Showing that the conditional diffusion model loss naturally emerges from an analysis of the black-box inversion problem.
2. Applying the resulting framework to invert face recognition models without identity-specific loss functions.
3. Demonstrating state-of-the-art performance in generating diverse, identity-preserving face images from black-box ID vectors.
4. Providing control mechanisms for the face recognition model inversion task.

## 2 Related work

### 2.1 Face recognition

While early deep learning works such as DeepFace [58] and VGG-Face [44] treated face recognition as a classification problem, with each class referring to one identity, FaceNet [52] introduced a new distance-based loss function: the triplet loss. The trend then shifted towards margin-based softmax methods that incorporate a margin penalty and perform sample-to-class comparisons rather than sample-to-sample comparisons [33, 63, 62, 10]. More recently, some FR methods tackle specific challenges such as robustness to different quality levels [27] and occlusions [31, 45].

### 2.2 Inversion of face recognition models

Similar to gradient-based feature visualization techniques [54, 34, 68, 39], Zhmoginov and Sandler [71] perform gradient ascent steps using the gradient of a pre-trained FR model to generate images that approach the same ID vector as a target image. To avoid generating adversarial examples, strong image priors such as a total-variation loss and the use of a guiding image are necessary. Cole *et al.* [4] transform the one-to-many task into a one-to-one task by mapping intermediate features of a FR model to frontal, neutral-expression images, enabling the use of an autoencoder architecture but requiring a difficult-to-obtain data set. Nitzan *et al.* [42] map the identity features and attributes of images into the style space of a pre-trained StyleGAN [24] to produce compelling results. However, their method struggles to encode real images since it is trained exclusively with images generated by StyleGAN. Furthermore, all of the above methods require white-box access to (the gradient of) a FR model, which is not always available in practice.

Many black-box methods view the problem from a security point-of-view, focusing on generating images that deceive a FR model rather than generating realistic faces with similar visual features. Early attempts using linear [38] or radial basis function models [37] lacked generative capacity to produce realistic images. NbNet [36] introduces a neighborly de-convolutional neural network that can generate images with a reasonable resemblance to a given image, but it has line artifacts and relies on a huge data set augmented with a GAN. On the contrary, Razzhigaev *et al.* [48] propose a data-set-free method using Gaussian blobs to produce images with ID vectors close to the target, but their results lack realism and take very long to generate due to querying the FR model hundreds of thousand times per image. Yang *et al.* [66] rely on background knowledge to invert a model and only produce blurry images in the black-box setting. Vec2Face [12] uses a new bijection metric and knowledge distillation from a black-box FR model to produce realistic identity-preserving faces; however, it requires a large data set (Casia-WebFace [67]) that contains multiple images of the same identity during training. Vendrow and Vendrow [61] take advantage of a pre-trained StyleGAN [24] generator to produce face images. They perform a random search in the StyleGAN latent space to find face images with an ID vector close to the target. While their method generates highly realistic images, the search strategy takes very long and often lands in local minima, resulting in images with completely different identities.

Table 1 compares attributes of state-of-the-art FR model inversion methods. Our method is the only one that does not suffer from any of the common shortcomings: It consistently generates diverse, realistic, identity-preserving images in the black-box setting, can be trained with easy-to-obtain data, and does not require access to the FR model during inference other than to obtain the ID vector of the target image.

Method	Black-box	Number of FR model queries during inference	Training data set	Realistic	Mapping
Zhmoginov and Sandler [71]	No	$\sim 1000^*$	Any images	No	One-to-one
Cole <i>et al.</i> [4]	No	1	Frontalized images	Yes	One-to-one
Nitzan <i>et al.</i> [42]	No	1	Any images	Yes	One-to-many
NbNet [36]	Yes	1	Huge data set	No	One-to-one
Gaussian sampling [48]	Yes	240000	Data-set-free	No	One-to-many
Yang <i>et al.</i> [66]	Yes	1	Any images	No	One-to-one
Vec2Face [12]	Yes	1	Multiple images per identity	Yes	One-to-many
StyleGAN search [61]	Yes	400	Data-set-free	Yes	One-to-many
ID3PM (Ours)	Yes	1	Any images	Yes	One-to-many

Table 1: Comparison of state-of-the-art face recognition (FR) model inversion methods. Our method does not have any of the common shortcomings, producing diverse, realistic images from black-box ID vectors with few requirements for the training data set or accessibility of the FR model during inference. \* The authors propose two methods: one taking hundreds or thousands of queries and the second one doing it in one shot.

### 3 Motivation

#### 3.1 Inverse problems

In a system under study, we often have a *forward problem* or function  $f$  that corresponds to a set of observations  $\mathbf{y} \sim \mathcal{Y}$ . The function  $f$  has input arguments  $\mathbf{x}$  and a set of parameters  $\theta$ , such that  $f(\mathbf{x}; \theta) = \mathbf{y}$ . An *inverse problem* seeks to reverse this process and make inferences about the values of  $\mathbf{x}$  or  $\theta$  given the observations  $\mathbf{y}$ . For the application explored in this work,  $f$  is a face recognition model that takes an image  $\mathbf{x}$  as input and produces an ID vector  $\mathbf{y}$ .

When the function  $f$  is not bijective, no inverse exists in the traditional mathematical sense. However, it is possible to generalize our concept of what an inverse is to accommodate the problem of model inversion, namely by considering an inverse to be the set of pre-images of the function  $f$  that map  $\epsilon$ -close to the target  $\mathbf{y}$ . For bijective  $f$ , this corresponds to the traditional inverse for  $\epsilon = 0$ .

##### 3.1.1 Model inversion with model access

A standard way to handle the model-inversion problem when  $f$  is not bijective is to treat it pointwise, defining a loss, such as

$$\mathcal{L} = \|\mathbf{y} - f(\mathbf{x})\|^2, \quad (1)$$

and minimizing it via gradient descent on  $\mathbf{x}$  from some starting point  $\mathbf{x}_0$ . One would then iteratively update an initial guess  $\mathbf{x}_0$  according to

$$\Delta \mathbf{x}_t = -\nabla_{\mathbf{x}} \mathcal{L} = \left( \frac{\partial f}{\partial \mathbf{x}} \right)^\top (\mathbf{y} - f(\mathbf{x})). \quad (2)$$

In common cases where the inverse problem is one-to-many, we can take a statistical approach. Here we want to sample from  $p(\mathbf{x}|\mathbf{y})$ , which is equivalent to drawing from the pre-image set that defines the inverse  $f^{-1}(\mathbf{y})$ .

However, if we assume a Gaussian observation model

$$p(\mathbf{y}|\mathbf{x}) = \mathcal{N}(\mathbf{y}; f(\mathbf{x}), \sigma^2 \mathbf{I}) \propto \exp \left( -\frac{\mathcal{L}}{2\sigma^2} \right), \quad (3)$$

where the last term follows from (1), then we can rewrite equation (2) as  $\Delta \mathbf{x}_t \propto \sigma^2 \nabla_{\mathbf{x}} \log p(\mathbf{y}|\mathbf{x}_t)$ .

This shows that traditional model inversion via gradient descent performs a type of deterministic sampling from  $p(\mathbf{y}|\mathbf{x})$ —and not the distribution we want,  $p(\mathbf{x}|\mathbf{y})$ —by pushing toward modes of  $p(\mathbf{y}|\mathbf{x})$  close to the initialization point  $\mathbf{x}_0$ , regardless of whether it possesses the desired characteristics of the data  $p(\mathbf{x})$ . This can lead to results, such as adversarial examples [15], that, while technically satisfying the mathematical criteria of inversion, do not appear to come from  $p(\mathbf{x})$ .

Various types of regularization exist to attempt to avoid this issue, which are most often *ad hoc* methods geared toward the specific problem at hand [71, 35, 5, 65]. A more general approach is to introduce regularization terms proportional to the (*Stein*) score,  $\nabla_{\mathbf{x}} \log p(\mathbf{x})$ , since

$$\nabla_{\mathbf{x}} \log p(\mathbf{x}|\mathbf{y}) = \nabla_{\mathbf{x}} \log p(\mathbf{y}|\mathbf{x}) + \nabla_{\mathbf{x}} \log p(\mathbf{x})$$

provides the *conditional* score needed to sample from  $p(\mathbf{x}|\mathbf{y})$ , the distribution we are actually interested in.

Previous work has shown that diffusion models effectively learn the score  $\nabla_{\mathbf{x}} \log p(\mathbf{x})$ , which allows them to be used alongside model gradients to guide sampling [56, 20, 41, 11, 23]. When those models are classifiers, the procedure is known as *classifier guidance* [11]. However, this imposes an additional computational burden on sampling and also requires that the model  $f$  be differentiable.

### 3.1.2 Model inversion without full model access

In the case we focus on in this work, we assume to have access only to the values of the function  $f$  via some oracle or a lookup table of  $(\mathbf{x}, \mathbf{y})$  pairs but not its gradient  $\nabla f$ . In this case, also referred to as *black-box* setting, we may wish to train a function  $g_\psi$  to learn the inverse by minimizing

$$\mathcal{J} = \|\mathbf{x} - g_\psi(\mathbf{y})\|^2 \quad (4)$$

across all observed  $\{(\mathbf{x}, \mathbf{y})\}$ . Recalling that  $\mathbf{y} = f(\mathbf{x})$ , we have essentially described an encoder-decoder setup with the encoder frozen and only the decoder being trained, which requires no gradients from the “encoder”  $f$ .

If we consider perturbed data  $\tilde{\mathbf{x}} = \mathbf{x} + \epsilon$ , where  $\epsilon \sim \mathcal{N}(\mathbf{0}, \sigma_t^2 \mathbf{I})$ . Then (4) is equivalent to

$$\begin{aligned} \tilde{\mathcal{J}} &= \|(\tilde{\mathbf{x}} - \mathbf{x}) - (\tilde{\mathbf{x}} - g_\psi(\mathbf{y}))\|^2 \\ &= \|\epsilon - \epsilon_\theta(\tilde{\mathbf{x}}, \mathbf{y}, t)\|^2, \end{aligned} \quad (5)$$

and we are now training a conditional model  $\epsilon_\theta$  to learn the noise added to  $\mathbf{x}$  instead of a model  $g$  to reconstruct  $\mathbf{x}$ . This new task is exactly the one facing conditional diffusion models (Section 4.1).

Although we cannot *force* the model to leverage the conditioning on  $\mathbf{y}$  or  $t$ , if it is to successfully minimize the loss  $\tilde{\mathcal{J}}$ , it should learn a function proportional to the conditional score. That is because, by Tweedie’s formula [13, 26],

$$\begin{aligned} \mathbb{E}[\mathbf{x}|\tilde{\mathbf{x}}, \mathbf{y}] &= \tilde{\mathbf{x}} + \sigma_t^2 \nabla_{\tilde{\mathbf{x}}} \log p(\tilde{\mathbf{x}}|\mathbf{y}) \\ &\approx \tilde{\mathbf{x}} - \epsilon_\theta(\tilde{\mathbf{x}}, \mathbf{y}, t). \end{aligned} \quad (6)$$

As a result, we can effectively sample from the “inverse distribution”  $p(\tilde{\mathbf{x}}|\mathbf{y})$  via  $\epsilon_\theta(\tilde{\mathbf{x}}, \mathbf{y}, t)$  using Langevin dynamics [1, 64] without having access to the gradients of the model  $f$  or any other model-specific loss terms.

## 4 Method

Motivated by the results from Sec. 3, we adopt a conditional diffusion model for the task of inverting a face recognition (FR) model. This results in a minimal formulation of the inverse problem compared to other methods that require complicated supervision [12] or regularization [71] signals. The overall architecture of our method, named identity denoising diffusion probabilistic model (ID3PM), is visualized in Fig. 2.

### 4.1 Diffusion model formulation

We build up on the diffusion model proposed by Dhariwal and Nichol [11]. Given a sample  $\mathbf{x}_0$  from the image distribution, a sequence  $\mathbf{x}_1, \mathbf{x}_2, \dots, \mathbf{x}_T$  of noisy images is produced by progressively adding Gaussian noise according to a variance schedule at each time step. At the final time step (say  $T = 1000$ ),  $\mathbf{x}_T$  is assumed to be pure Gaussian noise:  $\mathcal{N}(\mathbf{0}, \mathbf{I})$ . A neural network is then trained to reverse this diffusion process. In each training iteration, an image  $\mathbf{x}_0$  from the data set, and a time step  $t \in [1, T]$  are sampled, and the corrupted images  $\mathbf{x}_{t-1}$  and  $\mathbf{x}_t$  are produced. The model predicts  $\mathbf{x}_{t-1}$  (or rather a quantity from which  $\mathbf{x}_{t-1}$  can be obtained) given the noisy image  $\mathbf{x}_t$  and the time step  $t$ . For sampling a new image  $\mathbf{x}_0$ , we sample  $\mathbf{x}_T \sim \mathcal{N}(\mathbf{0}, \mathbf{I})$  and iteratively denoise it, producing a sequence  $\mathbf{x}_T, \mathbf{x}_{T-1}, \dots, \mathbf{x}_1, \mathbf{x}_0$ . The final image,  $\mathbf{x}_0$ , should resemble the training data.

As [11], we assume that we can model  $p_\theta(\mathbf{x}_{t-1}|\mathbf{x}_t)$  as a Gaussian  $\mathcal{N}(\mathbf{x}_{t-1}; \mu_\theta(\mathbf{x}_t, t), \Sigma_\theta(\mathbf{x}_t, t))$  whose mean  $\mu_\theta(\mathbf{x}_t, t)$  can be calculated as a function of  $\epsilon_\theta(\mathbf{x}_t, t)$ , the noise that corresponds to the difference between  $\mathbf{x}_t$  and  $\mathbf{x}_{t-1}$ . We extend this by conditioning on the ID vector  $\mathbf{y}$  and thus predict  $\epsilon_\theta(\mathbf{x}_t, \mathbf{y}, t)$ . Extending [41] to the conditional case, we elect to predict the noise  $\epsilon_\theta(\mathbf{x}_t, \mathbf{y}, t)$  and the variance  $\Sigma_\theta(\mathbf{x}_t, \mathbf{y}, t)$  from the image  $\mathbf{x}_t$ , the ID vector  $\mathbf{y}$ , and the time step  $t$ , using the objective

$$\mathcal{L}_{\text{simple}} = \mathbb{E}_{t, \mathbf{x}_0, \mathbf{y}, \epsilon} [\|\epsilon - \epsilon_\theta(\mathbf{x}_t, \mathbf{y}, t)\|^2]. \quad (7)$$

For more details, refer to the diffusion model works [20, 41, 11]. Note that this objective is identical to the one theoretically derived in (5). While some recent work has considered the application of diffusion models to inverse problems, they typically assume that  $p(\mathbf{y}|\mathbf{x})$  is known [56], while we make no such assumption.

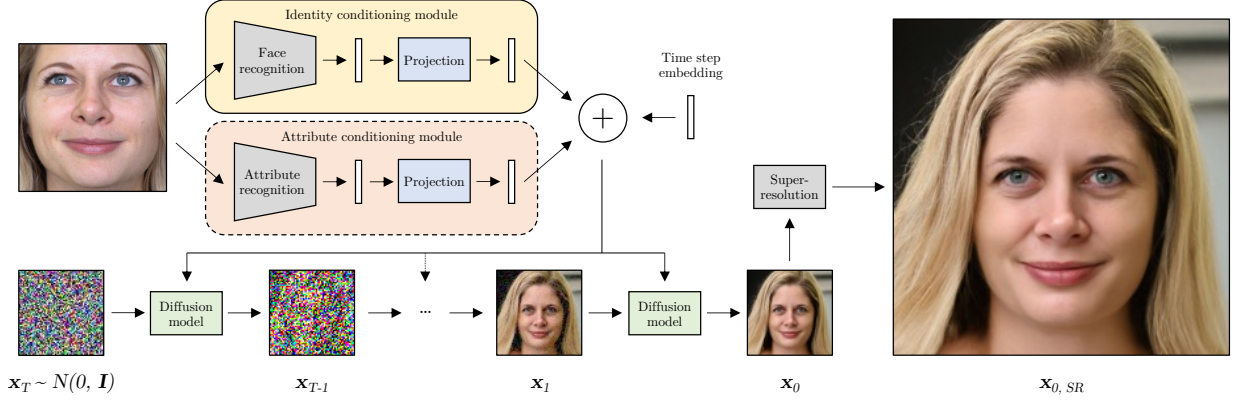


Figure 2: Method architecture. Given an image of a source identity, the identity conditioning module first extracts the ID vector with a black-box, pre-trained face recognition network. This is projected with a fully connected layer and added to the time step embedding which are both injected into the residual blocks of a diffusion model. Starting with Gaussian noise  $\mathbf{x}_T$ , the diffusion model iteratively denoises the image to finally obtain the output image  $\mathbf{x}_0$  in  $64 \times 64$  resolution after  $T$  diffusion time steps. Lastly, the image is upsampled to a resolution of  $256 \times 256$  using an unconditional super-resolution model, which is also a diffusion model. The optional attribute conditioning module helps disentangle identity-specific from identity-agnostic features and allows intuitive control over attributes such as the pose. Note that the gray components are not learned during training.

Following Ramesh *et al.* [47], we adapt classifier-free guidance [21] by setting the ID vector to the  $\mathbf{0}$ -vector every 10 batches during training. This effectively results in one model with two settings: conditional (ID vector) and unconditional ( $\mathbf{0}$ -vector). During inference, we sample from both settings, and the model prediction  $\hat{\epsilon}_\theta$  becomes

$$\hat{\epsilon}_\theta(\mathbf{x}_t, \mathbf{y}, t) = \epsilon_\theta(\mathbf{x}_t, \mathbf{0}, t) + s[\epsilon_\theta(\mathbf{x}_t, \mathbf{y}, t) - \epsilon_\theta(\mathbf{x}_t, \mathbf{0}, t)], \quad (8)$$

where  $s \geq 1$  is the guidance scale. Higher guidance scales cause the generation process to consider the identity conditioning more, effectively by re-weighting the balance of the conditional and unconditional scores.

## 4.2 Architecture

The architecture of the model is a U-net [49] that takes the image  $\mathbf{x}_t$ , the ID vector  $\mathbf{y}$ , and the time step  $t$  as input. The U-net architecture is adapted from [11] and is described in detail in Appendix A. To condition the diffusion model on the identity, we add an identity embedding to the residual connections of the ResNet blocks, as commonly done for class embeddings [11] and the CLIP [46] embedding in text-to-image generation methods [47, 50]. The identity embedding is obtained by projecting the ID vector through a learnable fully connected layer such that it has the same size as the time step embedding and can be added to it.

## 4.3 Controllability

Due to its robustness and ability to pick a mode by setting the random seed during image generation, our method permits smooth interpolations and analyses in the ID vector latent space unlike other works that invert FR models. For example, we can smoothly interpolate between different identities as visualized in Fig. 1. Furthermore, we can find meaningful directions in the latent spaces. Since the directions extracted automatically using principal component analysis (PCA) are generally difficult to interpret beyond the first dimension (see Appendix E.4), we calculate custom directions using publicly available metadata [6] for the FFHQ data set. For binary features (e.g. glasses), we define the custom direction vector as the difference between the mean ID vectors of the two groups. For continuous features (e.g. age), we map to the binary case by considering ID vectors with feature values below the 10th percentile and values above the 90th percentile for the two groups respectively. Examples of traveling along meaningful ID vector directions can be seen in Fig. 1.

To better disentangle identity and non-identity information and obtain additional interpretable control, we can optionally extend our method by also conditioning the diffusion model on an attribute vector as done for the ID vector. We form several sets of attributes grouped by how much they can be considered as part of a person’s identity (see Tab. 8). Set 1 only contains the emotion and head pose. Set 2 additionally contains glasses, makeup, and occlusions. Lastly, set 3 additionally contains age, facial hair, hair, and gender. As our method works with black-box vectors, it could be extended even more by simply adding more conditioning vectors.



#### 4.4 Implementation details

As data set, we use FFHQ [24] and split it into 69000 images for training and 1000 images for testing. Since we can only show images of individuals with written consent as explained in Sec. 6, we use a proprietary data set of faces for the qualitative results in this paper. To condition our model, we use ID vectors from Tim Esler’s PyTorch FaceNet implementation [14] or the default InsightFace method [8]. To evaluate the generated images and thereby match the verification accuracy on real images shown in Vec2Face [12] as closely as possible, we use the official PyTorch ArcFace implementation [7] and David Sandberg’s TensorFlow FaceNet implementation [51]. A detailed description of the remaining implementation details and ID vectors is in Appendix A.

## 5 Experiments and results

### 5.1 Comparison to state-of-the-art methods

We mainly compare our model with the three methods that generate faces from black-box features whose code is available online: NbNet [36] (“vgg-percept-nbnetb” parameters), the method by Razzhigaev *et al.* [48] (referred to as “Gaussian sampling”), and the method by Vendrow and Vendrow [61] (referred to as “StyleGAN search”).

Figure 3 compares the outputs of our method with those of current state-of-the-art methods. While capturing the identity of the input face well in some cases, NbNet [36] and Gaussian sampling [48] both fail to produce realistic faces. In contrast, StyleGAN search [61] always generates high-quality images, but they are not always faithful to the original identity, sometimes failing completely (by getting stuck in local minima) as seen in the last row. Our method is the only method that produces high-quality, realistic images that consistently resemble the original identity.

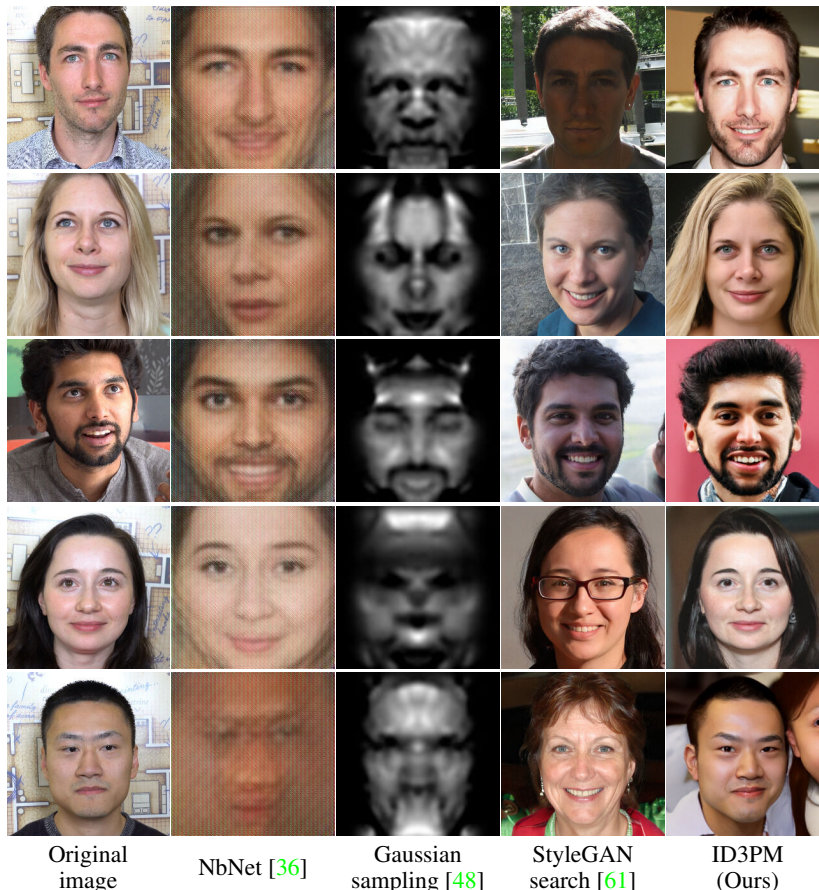


Figure 3: Qualitative evaluation with state-of-the-art methods. The generated images of our method (with InsightFace [8] ID vectors) look realistic and resemble the identity of the original image more closely than other methods. Note that the second-best performing method, StyleGAN search [61], often fails completely as seen in the last row.



For the quantitative evaluation of the identity preservation, we select all 1000 images from the FFHQ [24] test set and generate one image from each ID vector. We then calculate the distances according to the ArcFace [7] and FaceNet [51] face recognition methods for the 1000 pairs for each method. The resulting distributions of distances are plotted in Fig. 4. Note that StyleGAN search [61] optimizes the FaceNet distance during the image generation and thus performs well when evaluated with FaceNet but poorly when evaluated with ArcFace. The opposite effect can be seen for Gaussian sampling, which optimizes ArcFace during image generation. Despite not optimizing the ID vector distance directly (neither during training nor during inference), our method outperforms all other methods, producing images that are closer to the original images’ identities.

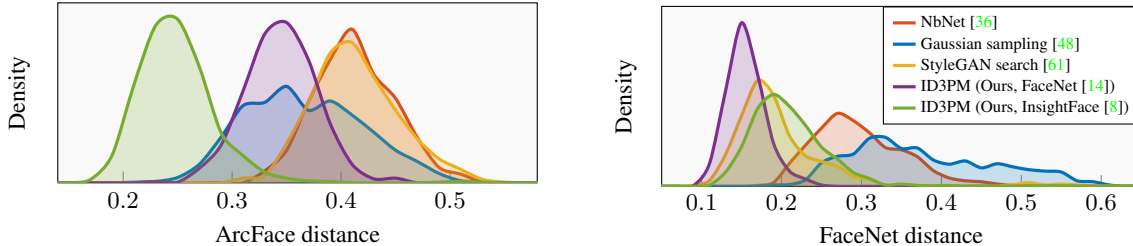


Figure 4: Probability density functions of the ArcFace [7] and FaceNet [51] distances of 1000 FFHQ [24] test images and their corresponding reconstructions.

To further evaluate the identity preservation and to compare to Vec2Face [12] despite their code not being available online, we follow the procedure used in Vec2Face [12]. Specifically, we use the official validation protocols of the LFW [22], AgeDB-30 [40], and CFP-FP [53] data sets and replace the first image in each positive pair with the image reconstructed from its ID vector, while keeping the second image as the real reference face. The face matching accuracies for ArcFace [7] and FaceNet [51] are reported in Tab. 2. Our method outperforms NbNet [36], Gaussian sampling [48], and StyleGAN search [61] in almost all tested configurations and performs on-par with or better than Vec2Face [12]. Note that our method has fewer requirements for the training data set (70000 face images instead of 490000 images grouped into 10000 classes) and produces visually superior results compared to Vec2Face [12].

Method	LFW		AgeDB-30		CFP-FP	
	ArcFace $\uparrow$	FaceNet $\uparrow$	ArcFace $\uparrow$	FaceNet $\uparrow$	ArcFace $\uparrow$	FaceNet $\uparrow$
Real images	99.83%	99.65%	98.23%	91.33%	98.86%	96.43%
NbNet [36]	87.32%	92.48%	81.83%	82.25%	87.36%	89.89%
Gaussian sampling [48] <sup>1</sup>	89.10%	75.07%	-	-	-	-
StyleGAN search [61] <sup>1</sup>	82.43%	95.45%	-	-	-	-
Vec2Face [12] <sup>2</sup>	99.13%	98.05%	93.53%	<b>89.80%</b>	89.03%	87.19%
ID3PM (Ours, FaceNet [14])	97.65%	<b>99.98%</b>	88.22%	88.00%	94.47%	<b>95.23%</b>
ID3PM (Ours, InsightFace [8])	<b>99.20%</b>	96.02%	<b>94.53%</b>	79.15%	<b>96.13%</b>	87.43%

Table 2: Quantitative evaluation of the identity preservation with state-of-the-art methods. The scores depict the matching accuracy when replacing one image of each positive pair with the image generated from its ID vector for the protocols of the LFW [22], AgeDB-30 [40], and CFP-FP [53] data sets. The best performing method per column is marked in bold. <sup>1</sup> The evaluation was not performed on AgeDB-30 and CFP-FP for the Gaussian sampling [48] and StyleGAN search [61] methods since it takes them several minutes to generate each image. <sup>2</sup> Values taken from their paper.

To evaluate the diversity of the generated results, we generate 100 images for the first 50 identities of the FFHQ [24] test set. Motivated by the diversity evaluation common in unpaired image-to-image translation literature [3, 30], we calculate the mean pairwise LPIPS [70] distances among all images of the same identity. We further calculate the mean pairwise pose and expressions extracted using 3DDFA\_V2 [17]. We additionally calculate the mean identity vector distances according to ArcFace [7] and FaceNet [51] to measure the identity preservation. We report these values in Tab. 3.

Since NbNet [36] is a one-to-one method and Gaussian sampling [48] produces faces that often fail to be detected by 3DDFA\_V2 [17], we only compare with StyleGAN search [61]. In our default configuration (marked with \* in Tab. 3), we obtain similar diversity scores as StyleGAN search [61], while preserving the identity much better. Note that part of

Method	Setting	Diversity			Identity distance	
		Pose $\uparrow$	Expression $\uparrow$	LPIPS $\uparrow$	ArcFace $\downarrow$	FaceNet $\downarrow$
StyleGAN search [61]	-	12.57	<b>1.57</b>	<b>0.317</b>	0.417	0.215
ID3PM (Ours) Guidance scales	1.0	17.36	1.35	0.315	0.291	0.234
	1.5	16.69	1.18	0.301	0.260	0.211
	2.0 *	16.24	1.10	0.290	0.247	0.203
	2.5	15.88	1.05	0.282	0.242	0.201
	3.0	15.55	1.01	0.274	<b>0.239</b>	<b>0.200</b>
ID3PM (Ours) Attribute sets	1	16.93	1.45	0.306	0.302	0.252
	2	17.21	1.51	0.299	0.289	0.246
	3	<b>18.35</b>	1.50	<b>0.317</b>	0.297	0.260

Table 3: Quantitative evaluation of the diversity and identity distances of 100 generated images for 50 identities with StyleGAN search [61], different guidance scales, and different attribute conditioning sets. InsightFace [8] ID vectors are used for all of our experiments. The best performing method per column is marked in bold. \* Indicates the default setting used in this paper and also for the runs with attribute conditioning.

the reason why StyleGAN search [61] performs well for the LPIPS [70] features is that the generated images often do not match the identity closely, as shown qualitatively in Fig. 8.

## 5.2 Controllability

### 5.2.1 Guidance scale

The classifier-free guidance scale offers us control over the trade-off between the fidelity and diversity of the generated results. As seen in Fig. 5, by increasing the guidance, the generated faces converge to the same identity, resemble the original face more closely, and contain fewer artifacts in the details. At the same time, higher guidance values reduce the diversity of non-identity-related features such as the background and expressions and also increase contrast and saturation.

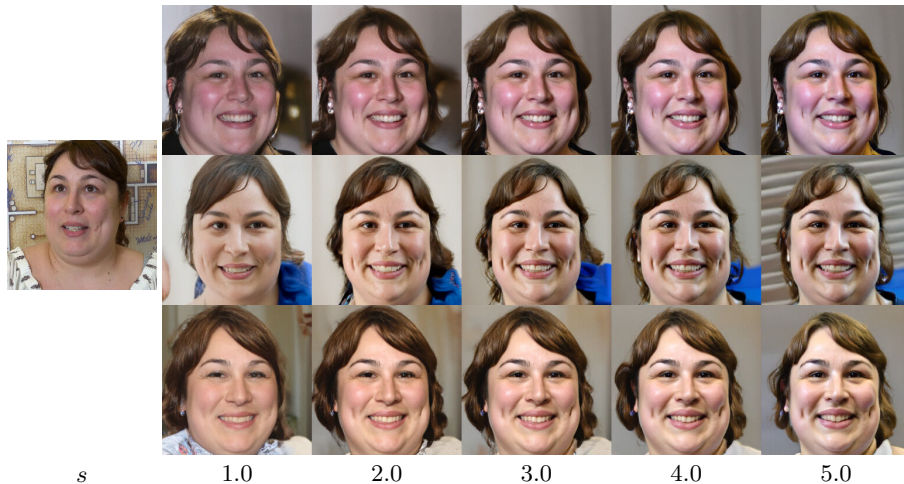


Figure 5: Effect of the guidance scale on the generated images. For the (InsightFace [8]) ID vector extracted from the image on the left, we generate images for four seeds at guidance scales  $s$  ranging from 1.0 to 5.0.

To measure this effect quantitatively, we perform the same evaluation as in the previous section and report the results in Tab. 3. As the guidance scale increases, the identity preservation improves as indicated by the decreasing identity distances, but the diversity in terms of poses, expressions, and LPIPS [70] features decreases. In practice, we choose a guidance scale of 2.0 for all experiments unless stated otherwise because that appears to be the best compromise between image quality and diversity. In Appendix C.1, we further calculate FID [19] as well as precision and recall [29] values to measure how well the image distribution is preserved as the guidance scale varies.

### 5.2.2 Identity vector latent space

As described in Sec. 4, we can find custom directions in the ID vector latent space that enable us to smoothly interpolate identities as well as change features such as the age or hair color as seen in Fig. 1 and in Appendix C.2. Note that we refer to these features as *identity-specific* because they exist in the ID vector latent space. In theory, this space should not contain any identity-agnostic information such as the pose. In practice, however, some FR methods inadvertently do extract this information. This is shown in great detail in Appendix E, where we show an interesting application of our method to analyze pre-trained face recognition methods.

### 5.2.3 Attribute conditioning

By additionally conditioning our method on attributes, we can disentangle identity-specific and identity-agnostic features. As seen in Fig. 6, the additional attribute conditioning allows us to recover more of the original data distribution in terms of head poses, expressions, and accessories whereas a model conditioned only on the ID vector is more likely to overfit and learn biases from the training data set. This is also shown in Tab. 3, where the diversity increases as the number of attributes increases at the expense of worse identity preservation compared to the base configuration. The attribute conditioning also enables intuitive control over the generated images by simply selecting the desired attribute values as shown in Fig. 1 and in Fig. 13.



Figure 6: Attribute conditioning diversity. Through additional attribute conditioning, we can disentangle identity and non-identity features. As a result, we obtain more diverse results when using both (InsightFace [8]) ID vector and attribute vector conditioning compared to when only using ID vector conditioning.

## 6 Ethical concerns and biases

All individuals portrayed in this paper provided informed consent to use their images as test images. This was not possible for the images from the FFHQ [24], LFW [22], AgeDB-30 [40], and CFP-FP [53] data sets. Therefore, we do not show them in the paper.

Our model inherits the biases of both the face recognition model and the training data set. This can manifest as either accessorizing images corresponding to certain demographic factors (*e.g.* via make-up, clothing) or losing identity fidelity for underrepresented groups. This suggests an additional application of our work to the study of systematic biases in otherwise black-box systems.

We recognize the potential for misuse of any method that creates realistic imagery of human beings, especially when the images are made to correspond to specific individuals. We condemn such misuse and support ongoing research into the identification of artificially manipulated data.

## 7 Conclusion

We propose a method to generate high-quality identity-preserving face images by injecting black-box, low-dimensional embeddings of a face into the residual blocks of a diffusion model. We mathematically reason and empirically show that our method produces images close to the target identity despite the absence of any identity-specific loss terms. Our method obtains state-of-the-art performance on identity preservation and output diversity, as demonstrated qualitatively and quantitatively. We further showcase advantages of our approach in providing control over the generation process. We thus provide a useful tool to create data sets with user-defined variations in identities and attributes as well as to analyze the latent spaces of face recognition methods, motivating more research in this direction.

## References

- [1] Giovanni Bussi and Michele Parrinello. Accurate sampling using langevin dynamics. *Physical Review E*, 75(5):056707, 2007.
- [2] Renwang Chen, Xuanhong Chen, Bingbing Ni, and Yanhao Ge. Simswap: An efficient framework for high fidelity face swapping. In *Proceedings of the 28th ACM International Conference on Multimedia*, pages 2003–2011, 2020.
- [3] Yunjey Choi, Youngjung Uh, Jaejun Yoo, and Jung-Woo Ha. Stargan v2: Diverse image synthesis for multiple domains. In *Proceedings of the IEEE/CVF conference on computer vision and pattern recognition*, pages 8188–8197, 2020.
- [4] Forrester Cole, David Belanger, Dilip Krishnan, Aaron Sarna, Inbar Mosseri, and William T Freeman. Synthesizing normalized faces from facial identity features. In *Proceedings of the IEEE conference on computer vision and pattern recognition*, pages 3703–3712, 2017.
- [5] Antonia Creswell and Anil Anthony Bharath. Inverting the generator of a generative adversarial network. *IEEE transactions on neural networks and learning systems*, 30(7):1967–1974, 2018.
- [6] DCGM. Gender, age, and emotions extracted for flickr-faces-hq dataset (ffhq), 2020.
- [7] Jinakang Deng, Jia Guo, Xiang An, Jack Yu, and Baris Gecer. Distributed arcface training in pytorch, 2021.
- [8] Jinakang Deng, Jia Guo, Xiang An, Jack Yu, and Baris Gecer. Insightface: 2d and 3d face analysis project, 2022.
- [9] Jiankang Deng, Jia Guo, Evangelos Ververas, Irene Kotsia, and Stefanos Zafeiriou. Retinaface: Single-shot multi-level face localisation in the wild. In *Proceedings of the IEEE/CVF conference on computer vision and pattern recognition*, pages 5203–5212, 2020.
- [10] Jiankang Deng, Jia Guo, Niannan Xue, and Stefanos Zafeiriou. Arcface: Additive angular margin loss for deep face recognition. In *Proceedings of the IEEE/CVF conference on computer vision and pattern recognition*, pages 4690–4699, 2019.
- [11] Prafulla Dhariwal and Alexander Nichol. Diffusion models beat gans on image synthesis. *Advances in Neural Information Processing Systems*, 34:8780–8794, 2021.
- [12] Chi Nhan Duong, Thanh-Dat Truong, Khoa Luu, Kha Gia Quach, Hung Bui, and Kaushik Roy. Vec2face: Unveil human faces from their blackbox features in face recognition. In *Proceedings of the IEEE/CVF Conference on Computer Vision and Pattern Recognition*, pages 6132–6141, 2020.
- [13] Bradley Efron. Tweedie’s formula and selection bias. *Journal of the American Statistical Association*, 106(496):1602–1614, 2011.
- [14] Tim Esler. Face recognition using pytorch, 2021.
- [15] Ian J Goodfellow, Jonathon Shlens, and Christian Szegedy. Explaining and harnessing adversarial examples. *arXiv preprint arXiv:1412.6572*, 2014.
- [16] Gaurav Goswami, Nalini Ratha, Akshay Agarwal, Richa Singh, and Mayank Vatsa. Unravelling robustness of deep learning based face recognition against adversarial attacks. In *Proceedings of the AAAI Conference on Artificial Intelligence*, volume 32, 2018.
- [17] Jianzhu Guo, Xiangyu Zhu, Yang Yang, Fan Yang, Zhen Lei, and Stan Z Li. Towards fast, accurate and stable 3d dense face alignment. In *Computer Vision–ECCV 2020: 16th European Conference, Glasgow, UK, August 23–28, 2020, Proceedings, Part XIX*, pages 152–168. Springer, 2020.
- [18] Kaiming He, Xiangyu Zhang, Shaoqing Ren, and Jian Sun. Deep residual learning for image recognition. In *Proceedings of the IEEE conference on computer vision and pattern recognition*, pages 770–778, 2016.
- [19] Martin Heusel, Hubert Ramsauer, Thomas Unterthiner, Bernhard Nessler, and Sepp Hochreiter. Gans trained by a two time-scale update rule converge to a local nash equilibrium. *Advances in neural information processing systems*, 30, 2017.
- [20] Jonathan Ho, Ajay Jain, and Pieter Abbeel. Denoising diffusion probabilistic models. *Advances in Neural Information Processing Systems*, 33:6840–6851, 2020.
- [21] Jonathan Ho and Tim Salimans. Classifier-free diffusion guidance. *arXiv preprint arXiv:2207.12598*, 2022.
- [22] Gary B Huang, Marwan Mattar, Tamara Berg, and Eric Learned-Miller. Labeled faces in the wild: A database for studying face recognition in unconstrained environments. In *Workshop on faces in ‘Real-Life’ Images: detection, alignment, and recognition*, 2008.
- [23] Tero Karras, Miika Aittala, Timo Aila, and Samuli Laine. Elucidating the design space of diffusion-based generative models. *arXiv preprint arXiv:2206.00364*, 2022.
- [24] Tero Karras, Samuli Laine, and Timo Aila. A style-based generator architecture for generative adversarial networks. In *Proceedings of the IEEE/CVF conference on computer vision and pattern recognition*, pages 4401–4410, 2019.
- [25] Jiseob Kim, Jihoon Lee, and Byoung-Tak Zhang. Smooth-swap: a simple enhancement for face-swapping with smoothness. In *Proceedings of the IEEE/CVF Conference on Computer Vision and Pattern Recognition*, pages 10779–10788, 2022.

- [26] Kwanyoung Kim and Jong Chul Ye. Noise2score: tweedie’s approach to self-supervised image denoising without clean images. *Advances in Neural Information Processing Systems*, 34:864–874, 2021.
- [27] Minchul Kim, Anil K Jain, and Xiaoming Liu. Adaface: Quality adaptive margin for face recognition. In *Proceedings of the IEEE/CVF Conference on Computer Vision and Pattern Recognition*, pages 18750–18759, 2022.
- [28] Adam Kortylewski, Bernhard Egger, Andreas Schneider, Thomas Gerig, Andreas Morel-Forster, and Thomas Vetter. Empirically analyzing the effect of dataset biases on deep face recognition systems. In *Proceedings of the IEEE conference on computer vision and pattern recognition workshops*, pages 2093–2102, 2018.
- [29] Tuomas Kynkäänniemi, Tero Karras, Samuli Laine, Jaakko Lehtinen, and Timo Aila. Improved precision and recall metric for assessing generative models. *Advances in Neural Information Processing Systems*, 32, 2019.
- [30] Hsin-Ying Lee, Hung-Yu Tseng, Qi Mao, Jia-Bin Huang, Yu-Ding Lu, Maneesh Singh, and Ming-Hsuan Yang. Dri++: Diverse image-to-image translation via disentangled representations. *International Journal of Computer Vision*, 128:2402–2417, 2020.
- [31] Chenyu Li, Shiming Ge, Daichi Zhang, and Jia Li. Look through masks: Towards masked face recognition with de-occlusion distillation. In *Proceedings of the 28th ACM International Conference on Multimedia*, pages 3016–3024, 2020.
- [32] Chang Liu, Xiang Yu, Yi-Hsuan Tsai, Masoud Faraki, Ramin Moslemi, Manmohan Chandraker, and Yun Fu. Learning to learn across diverse data biases in deep face recognition. In *Proceedings of the IEEE/CVF Conference on Computer Vision and Pattern Recognition*, pages 4072–4082, 2022.
- [33] Weiyang Liu, Yandong Wen, Zhiding Yu, Ming Li, Bhiksha Raj, and Le Song. Sphreface: Deep hypersphere embedding for face recognition. In *Proceedings of the IEEE conference on computer vision and pattern recognition*, pages 212–220, 2017.
- [34] Aravindh Mahendran and Andrea Vedaldi. Understanding deep image representations by inverting them. In *Proceedings of the IEEE conference on computer vision and pattern recognition*, pages 5188–5196, 2015.
- [35] Aravindh Mahendran and Andrea Vedaldi. Understanding deep image representations by inverting them. In *Proceedings of the IEEE conference on computer vision and pattern recognition*, pages 5188–5196, 2015.
- [36] Guangcan Mai, Kai Cao, Pong C Yuen, and Anil K Jain. Face image reconstruction from deep templates. *arXiv preprint arXiv:1703.00832*, 2017.
- [37] Alexis Mignon and Frédéric Jurie. Reconstructing faces from their signatures using rbf regression. In *British Machine Vision Conference 2013*, pages 103–1, 2013.
- [38] Pranab Mohanty, Sudeep Sarkar, and Rangachar Kasturi. From scores to face templates: A model-based approach. *IEEE transactions on pattern analysis and machine intelligence*, 29(12):2065–2078, 2007.
- [39] Alexander Mordvintsev, Christopher Olah, and Mike Tyka. Inceptionism: Going deeper into neural networks. 2015.
- [40] Stylianos Moschoglou, Athanasios Papaioannou, Christos Sagonas, Jiankang Deng, Irene Kotsia, and Stefanos Zafeiriou. Agedb: the first manually collected, in-the-wild age database. In *proceedings of the IEEE conference on computer vision and pattern recognition workshops*, pages 51–59, 2017.
- [41] Alexander Quinn Nichol and Prafulla Dhariwal. Improved denoising diffusion probabilistic models. In *International Conference on Machine Learning*, pages 8162–8171. PMLR, 2021.
- [42] Yotam Nitzan, Amit Bermano, Yangyan Li, and Daniel Cohen-Or. Face identity disentanglement via latent space mapping. *arXiv preprint arXiv:2005.07728*, 2020.
- [43] OpenAI. guided-diffusion, 2021.
- [44] Omkar M Parkhi, Andrea Vedaldi, and Andrew Zisserman. Deep face recognition. In *British Machine Vision Association*, 2015.
- [45] Haibo Qiu, Dihong Gong, Zhifeng Li, Wei Liu, and Dacheng Tao. End2end occluded face recognition by masking corrupted features. *IEEE Transactions on Pattern Analysis and Machine Intelligence*, 2021.
- [46] Alec Radford, Jong Wook Kim, Chris Hallacy, Aditya Ramesh, Gabriel Goh, Sandhini Agarwal, Girish Sastry, Amanda Askell, Pamela Mishkin, Jack Clark, et al. Learning transferable visual models from natural language supervision. In *International Conference on Machine Learning*, pages 8748–8763. PMLR, 2021.
- [47] Aditya Ramesh, Prafulla Dhariwal, Alex Nichol, Casey Chu, and Mark Chen. Hierarchical text-conditional image generation with clip latents. *arXiv preprint arXiv:2204.06125*, 2022.
- [48] Anton Razzhigaev, Klim Kireev, Edgar Kaziakhmedov, Nurislam Tursynbek, and Aleksandr Petiushko. Black-box face recovery from identity features. In *European Conference on Computer Vision*, pages 462–475. Springer, 2020.
- [49] Olaf Ronneberger, Philipp Fischer, and Thomas Brox. U-net: Convolutional networks for biomedical image segmentation. In *International Conference on Medical image computing and computer-assisted intervention*, pages 234–241. Springer, 2015.



- [50] Chitwan Saharia, William Chan, Saurabh Saxena, Lala Li, Jay Whang, Emily Denton, Seyed Kamyar Seyed Ghasemipour, Burcu Karagol Ayan, S Sara Mahdavi, Rapha Gontijo Lopes, et al. Photorealistic text-to-image diffusion models with deep language understanding. *arXiv preprint arXiv:2205.11487*, 2022.
- [51] David Sandberg. Face recognition using tensorflow, 2018.
- [52] Florian Schroff, Dmitry Kalenichenko, and James Philbin. Facenet: A unified embedding for face recognition and clustering. In *Proceedings of the IEEE conference on computer vision and pattern recognition*, pages 815–823, 2015.
- [53] Soumyadip Sengupta, Jun-Cheng Chen, Carlos Castillo, Vishal M Patel, Rama Chellappa, and David W Jacobs. Frontal to profile face verification in the wild. In *2016 IEEE winter conference on applications of computer vision (WACV)*, pages 1–9. IEEE, 2016.
- [54] Karen Simonyan, Andrea Vedaldi, and Andrew Zisserman. Deep inside convolutional networks: Visualising image classification models and saliency maps. *arXiv preprint arXiv:1312.6034*, 2013.
- [55] Richa Singh, Akshay Agarwal, Maneet Singh, Shruti Nagpal, and Mayank Vatsa. On the robustness of face recognition algorithms against attacks and bias. In *Proceedings of the AAAI Conference on Artificial Intelligence*, volume 34, pages 13583–13589, 2020.
- [56] Yang Song, Jascha Sohl-Dickstein, Diederik P Kingma, Abhishek Kumar, Stefano Ermon, and Ben Poole. Score-based generative modeling through stochastic differential equations. *arXiv preprint arXiv:2011.13456*, 2020.
- [57] Yi Sun, Yuheng Chen, Xiaogang Wang, and Xiaoou Tang. Deep learning face representation by joint identification-verification. *Advances in neural information processing systems*, 27, 2014.
- [58] Yaniv Taigman, Ming Yang, Marc’Aurelio Ranzato, and Lior Wolf. Deepface: Closing the gap to human-level performance in face verification. In *Proceedings of the IEEE conference on computer vision and pattern recognition*, pages 1701–1708, 2014.
- [59] Philipp Terhörst, Jan Niklas Kolf, Marco Huber, Florian Kirchbuchner, Naser Damer, Aythami Morales Moreno, Julian Fierrez, and Arjan Kuijper. A comprehensive study on face recognition biases beyond demographics. *IEEE Transactions on Technology and Society*, 3(1):16–30, 2021.
- [60] Ashish Vaswani, Noam Shazeer, Niki Parmar, Jakob Uszkoreit, Llion Jones, Aidan N Gomez, Łukasz Kaiser, and Illia Polosukhin. Attention is all you need. *Advances in neural information processing systems*, 30, 2017.
- [61] Edward Vendrow and Joshua Vendrow. Realistic face reconstruction from deep embeddings. In *NeurIPS 2021 Workshop Privacy in Machine Learning*, 2021.
- [62] Feng Wang, Jian Cheng, Weiyang Liu, and Haijun Liu. Additive margin softmax for face verification. *IEEE Signal Processing Letters*, 25(7):926–930, 2018.
- [63] Hao Wang, Yitong Wang, Zheng Zhou, Xing Ji, Dihong Gong, Jingchao Zhou, Zhifeng Li, and Wei Liu. Cosface: Large margin cosine loss for deep face recognition. In *Proceedings of the IEEE conference on computer vision and pattern recognition*, pages 5265–5274, 2018.
- [64] Max Welling and Yee W Teh. Bayesian learning via stochastic gradient langevin dynamics. In *Proceedings of the 28th international conference on machine learning (ICML-11)*, pages 681–688, 2011.
- [65] Weihao Xia, Yulun Zhang, Yujiu Yang, Jing-Hao Xue, Bolei Zhou, and Ming-Hsuan Yang. Gan inversion: A survey. *IEEE Transactions on Pattern Analysis and Machine Intelligence*, 2022.
- [66] Ziqi Yang, Jiyi Zhang, Ee-Chien Chang, and Zhenkai Liang. Neural network inversion in adversarial setting via background knowledge alignment. In *Proceedings of the 2019 ACM SIGSAC Conference on Computer and Communications Security, CCS ’19*, pages 225–240, New York, NY, USA, 2019. ACM.
- [67] Dong Yi, Zhen Lei, Shengcai Liao, and Stan Z Li. Learning face representation from scratch. *arXiv preprint arXiv:1411.7923*, 2014.
- [68] Jason Yosinski, Jeff Clune, Anh Nguyen, Thomas Fuchs, and Hod Lipson. Understanding neural networks through deep visualization. *arXiv preprint arXiv:1506.06579*, 2015.
- [69] Kaipeng Zhang, Zhanpeng Zhang, Zhifeng Li, and Yu Qiao. Joint face detection and alignment using multitask cascaded convolutional networks. *IEEE signal processing letters*, 23(10):1499–1503, 2016.
- [70] Richard Zhang, Phillip Isola, Alexei A Efros, Eli Shechtman, and Oliver Wang. The unreasonable effectiveness of deep features as a perceptual metric. In *Proceedings of the IEEE conference on computer vision and pattern recognition*, pages 586–595, 2018.
- [71] Andrey Zhmoginov and Mark Sandler. Inverting face embeddings with convolutional neural networks. *arXiv preprint arXiv:1606.04189*, 2016.

## A Additional implementation details

**ID vectors** Table 4 lists the face recognition methods used in this work. Note that we use two implementations for ArcFace [10] and FaceNet [52], one for training and the other one for evaluation in each case. The methods used for evaluation were chosen to match the verification accuracy on real images as closely as possible to the values shown in Vec2Face [12] to enable a fair comparison. For both evaluation methods, we extract the identity embeddings for each image as well as its horizontally flipped version and then calculate the angular distance of the concatenated identity embeddings after subtracting the mean embedding, similar to David Sandberg’s implementation [51]. In order to avoid having the face detector stage of different face recognition vectors influence the qualitative results, we manually confirmed that all shown test images were properly aligned.

Method	Usage	Alignment	Implementation	Checkpoint
AdaFace [27]	Training *	Provided MTCNN [69]	Official GitHub repository	“adaface_ir50_ms1mv2.ckpt”
ArcFace [10]	Evaluation	RetinaFace [9] from [8]	Official GitHub repository	“ms1mv3_arcface_r100_fp16”
ArcFace [10]	Training *	MTCNN [69] from [14]	From Razzhigayev <i>et al.</i> [48]	“torchtest.pt”
FaceNet [52]	Evaluation	Provided MTCNN [69]	From David Sandberg [51]	“20180402-114759”
FaceNet [52]	Training	Provided MTCNN [69]	From Tim Esler [14]	“20180402-114759”
FROM [45]	Training *	MTCNN [69] from [14]	Official GitHub repository	“model_p5_w1_9938_9470_6503.pth.tar”
InsightFace	Training	Provided RetinaFace [9]	InsightFace repository [8]	“buffalo_l”

Table 4: Overview over the considered face recognition methods. \* Only used in Appendix E.

**Model** We use the official U-net [49] implementation by Dhariwal and Nichol [11, 43] and their recommended hyperparameters, whenever applicable, for the main  $64 \times 64$  ID-conditioned face generation model and the  $64 \rightarrow 256$  super-resolution model as listed in Tab. 5. The U-net architecture is divided into several levels, with each level composed of ResNet [18] blocks and down- or upsampling layers. The U-net also contains global attention layers at  $32 \times 32$ ,  $16 \times 16$ , and  $8 \times 8$  resolutions. The time step  $t$  is passed through a sinusoidal position embedding layer, known from transformers [60], and is then added to the residual connection of the ResNet blocks. The most important additions to the baseline model are the identity conditioning module (identity\_cond) and introducing classifier-free guidance (classifier\_free) by setting the conditioning vector to the 0-vector<sup>2</sup> for 10% of the training iterations to obtain an unconditional and conditional setting with just one trained model.

**Training** The training set is composed of images along with their corresponding (pre-computed) ID vectors. We train the  $64 \times 64$  ID-conditioned face generation model for 100000 batches and the  $64 \times 64$  unconditional upsampling model for 50000 batches, both with a batch size of 64, learning rate of  $10^{-4}$ , and from scratch. We use the weights with an exponential moving average rate of 0.9999 because it generally leads to better results. Training takes around two days on one NVIDIA RTX 3090 GPU.

**Inference** All models are trained with  $T = 1000$  but respaced to 250 time steps during inference for computational reasons with a negligible decrease in quality. We use a classifier-free guidance scale of 2 unless otherwise stated. Furthermore, we fix the randomness seeds whenever comparing different methods to ensure a fair comparison. Inference (main model + super-resolution to  $256 \times 256$  resolution) takes around four minutes for a batch of 16 images on one NVIDIA RTX 3090 GPU.

<sup>2</sup>For attribute conditioning, the  $-1$ -vector is used since the 0-vector is a valid attribute vector (*e.g.* age 0) and the  $-1$ -vector performed better empirically.

	$64 \times 64$ Main model	$64 \times 64 \rightarrow 256 \times 256$ Super-resolution model
<u>Diffusion parameters</u>		
diffusion_steps	1000	1000
noise_schedule	cosine	linear
<u>Model parameters</u>		
attention_resolutions	32, 16, 8	32, 16, 8
classifier_free	True	False
dropout	0.1	0
identity_cond	True	False
learn_sigma	True	True
num_channels	192	192
num_heads	3	4
num_res_blocks	3	2
resblock_updown	True	True
use_fp16	True	True
use_new_attention_order	True	False
use_scale_shift_norm	True	True
<u>Training parameters</u>		
batch_size	64	64
ema_rate	0.9999	0.9999
lr (learning rate)	$10^{-4}$	$10^{-4}$
total_steps (batches)	100000	50000

Table 5: Hyperparameters of our diffusion models. We use one diffusion model to generate  $64 \times 64$  resolution images and one super-resolution diffusion model to increase the resolution to  $256 \times 256$ . All other parameters are named as in the baseline implementation (where applicable).

## B Additional qualitative comparisons to state-of-the-art methods

Figure 7 shows additional results of the qualitative comparison with the state-of-the-art black-box methods, whose code is available, and demonstrates the superiority of our method both in terms of image quality and identity preservation.

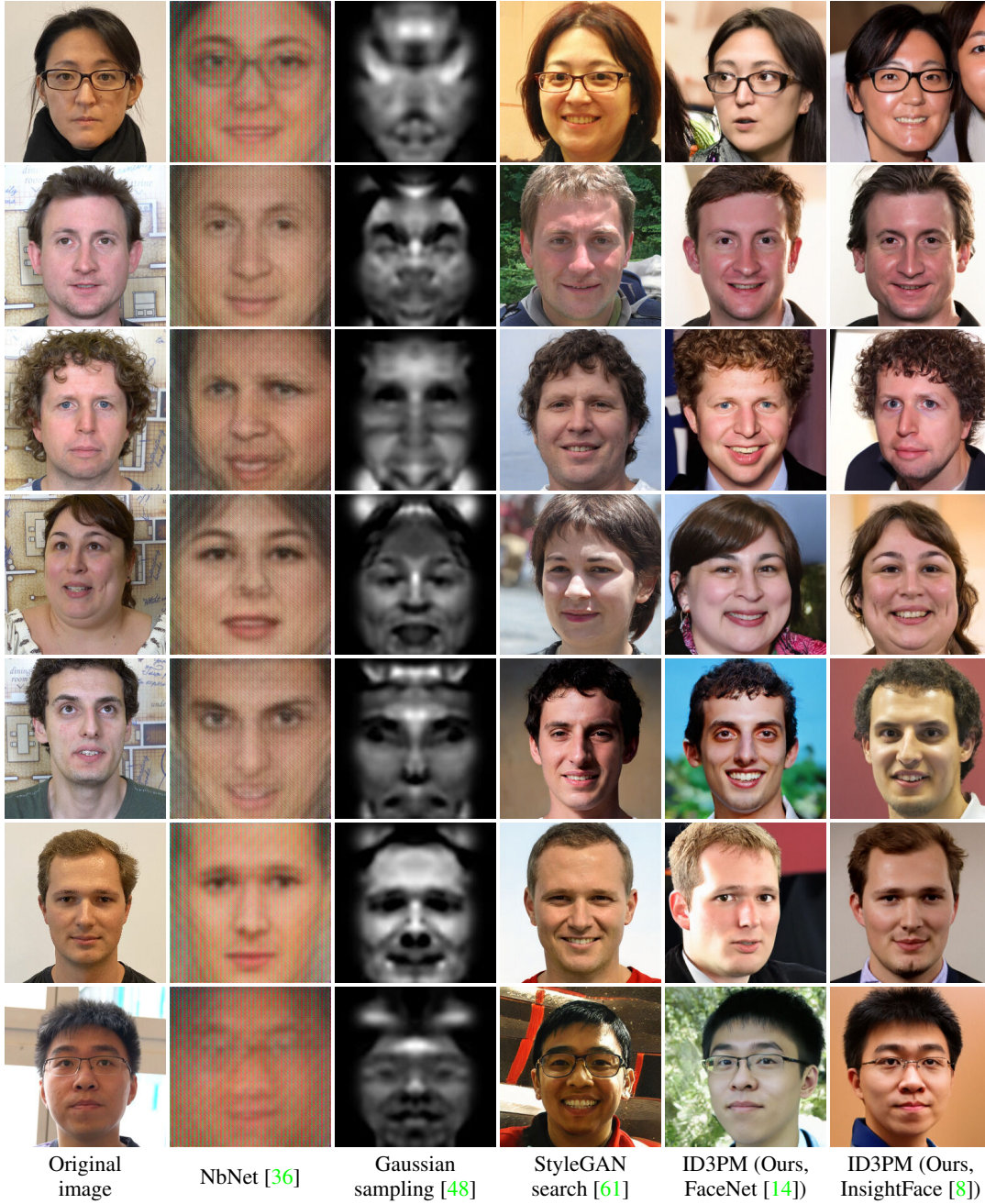


Figure 7: Qualitative evaluation with state-of-the-art methods (additional results). The generated images of our method look realistic and resemble the identity of the original image more closely than any of the other methods.



In Tab. 3, we quantitatively compare the diversity of our method with that of StyleGAN search [61], which is the only competing method that can produce realistic images at a high resolution. Figure 8 qualitatively confirms that our method produces similarly diverse images but with better identity preservation. For fairness reasons, we use our model trained with FaceNet [14] ID vectors since StyleGAN search [61] uses the same FaceNet [14] implementation. For the first two identities, the StyleGAN search [61] algorithm finds images that share facial features with the original face; however, the identity does not resemble the original face very closely. For the third identity, the search strategy often fails completely by landing in local minima.



Figure 8: Qualitative evaluation with StyleGAN search [61]. The generated images of our method resemble the identity of the original image closely and more consistently. Note that StyleGAN search [61] often fails completely for the third identity, whereas our method trained with the same face recognition method (FaceNet [14]) reproduces the identity well.



## C Controllability

To the best of our knowledge, our method is the first black-box face recognition model inversion method that offers intuitive control over the generation process. The mechanisms described in the following section enable the generation of data sets with control over variation and diversity of the identities as well as their attributes.

### C.1 Guidance scale

As described in Sec. 5.2.1, the guidance scale of the classifier-free guidance controls the trade-off between the fidelity in terms of identity preservation (higher guidance) and the diversity of the generated faces (lower guidance). Figure 9 shows examples of the generated images for different guidance scales  $s$  ranging from 1.0 to 5.0. To improve the performance for high guidance scales, we adopt dynamic thresholding from Imagen [50] with a threshold of 0.99.

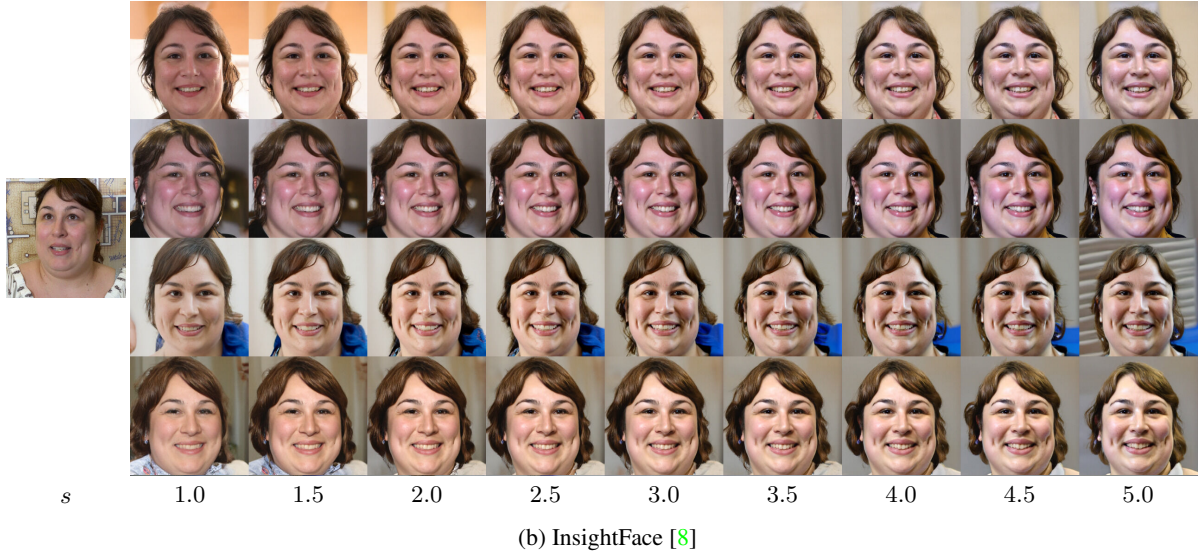
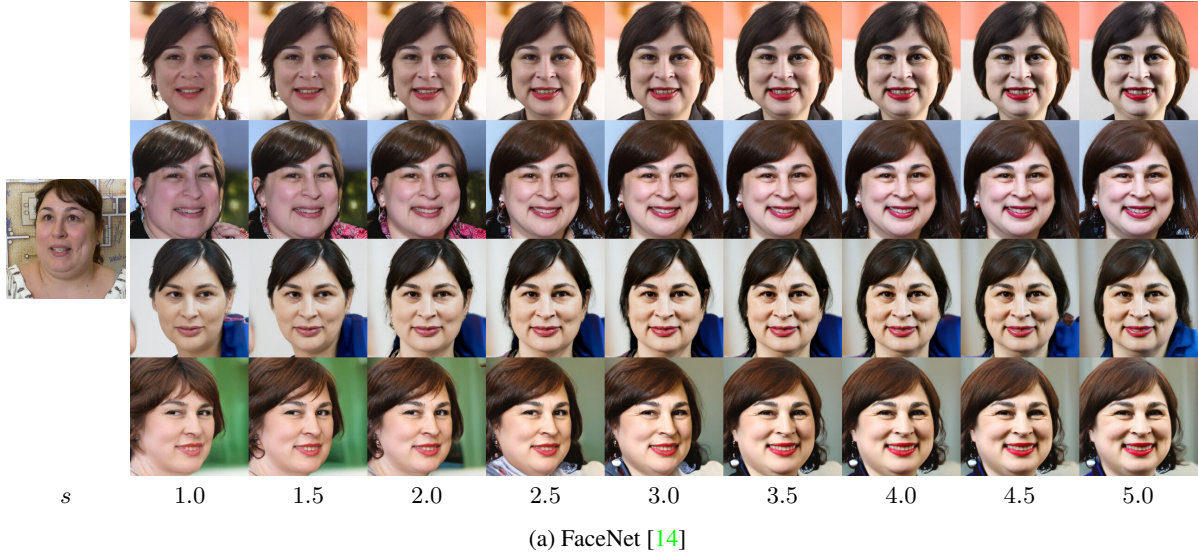


Figure 9: Qualitative evaluation of the effect of the guidance scale. For each ID vector extracted from the image on the left, we generate images for four seeds at guidance scales  $s$  ranging from 1.0 to 5.0.

In Tab. 3, we evaluate the diversity in terms of the pairwise pose, expression, and LPIPS [70] feature distances among generated images as well as their identity embedding distances. To further quantify the effect of the guidance, we select the first 10000 images of the FFHQ data set [24], extract their ID vectors, and generate one image for each ID vector<sup>3</sup>. These 10000 images are then compared to the corresponding 10000 original images in terms of their FID scores [19] as well as precision and recall [29]. The results are shown in Tab. 6. The precision score assesses to which extent the generated samples fall into the distribution of the the real images. Guidance scales in the range  $s = 1.5$  to  $s = 2.0$  raise the precision score, implying a higher image quality of the generated images. Even larger guidance scales lead to lower precision scores, which could be explained by the saturated colors observed in Fig. 9. The recall score measures how much of the original distribution is covered by the generated samples and corresponds to the diversity. As the guidance scale increases, recall decreases. Similarly, the FID score gets worse with higher guidance scales, demonstrating the decrease in diversity among the generated images.

Method ID vector	Guidance scale $s$	FID ( $\downarrow$ )	Precision ( $\uparrow$ )	Recall ( $\uparrow$ )
ID3PM (Ours, FaceNet [14])	1.0	<b>8.014</b>	0.768	<b>0.498</b>
	1.5	9.141	0.782	0.490
	2.0	10.434	<b>0.783</b>	0.476
	2.5	11.659	0.775	0.452
	3.0	12.806	0.771	0.441
ID3PM (Ours, InsightFace [8])	1.0	<b>6.786</b>	0.774	<b>0.517</b>
	1.5	7.442	<b>0.782</b>	0.516
	2.0	8.497	0.771	0.508
	2.5	9.286	0.763	0.506
	3.0	10.119	0.746	0.488

Table 6: Quantitative evaluation of the effect of the guidance scale on image quality and diversity. The best performing setting for each ID vector is marked in bold.

Additionally, we perform the face verification experiment from Tab. 2 on LFW [22], AgeDB-30 [40], and CFP-FP [53] with guidance scales between 1.0 and 3.0 for our models trained using FaceNet [14] and InsightFace [8] ID vectors. As seen in Tab. 7, the face verification accuracy generally increases with higher guidance scales but saturates eventually, confirming our qualitative findings that the guidance aids in the identity preservation.

Method	Guidance scale $s$	LFW		AgeDB-30		CFP-FP	
		ArcFace $\uparrow$	FaceNet $\uparrow$	ArcFace $\uparrow$	FaceNet $\uparrow$	ArcFace $\uparrow$	FaceNet $\uparrow$
Real images	-	99.83%	99.65%	98.23%	91.33%	98.86%	96.43%
ID3PM (Ours, FaceNet [14])	1.0	95.60%	98.62%	84.07%	86.20%	91.83%	94.30%
	1.5	97.08%	99.00%	87.55%	87.90%	94.20%	95.04%
	2.0	97.65%	98.98%	88.22%	88.00%	94.47%	<b>95.23%</b>
	2.5	97.92%	98.92%	<b>88.75%</b>	<b>88.47%</b>	<b>94.61%</b>	95.19%
	3.0	<b>98.03%</b>	<b>99.07%</b>	88.45%	<b>88.47%</b>	94.47%	95.03%
ID3PM (Ours, InsightFace [8])	1.0	98.38%	94.37%	91.88%	75.60%	93.50%	85.26%
	1.5	98.95%	95.62%	93.88%	77.57%	95.59%	86.81%
	2.0	<b>99.20%</b>	96.02%	94.53%	79.15%	96.13%	87.43%
	2.5	98.97%	<b>96.37%</b>	<b>94.88%</b>	79.20%	96.03%	87.83%
	3.0	99.15%	96.30%	94.78%	<b>79.25%</b>	<b>96.16%</b>	<b>87.97%</b>

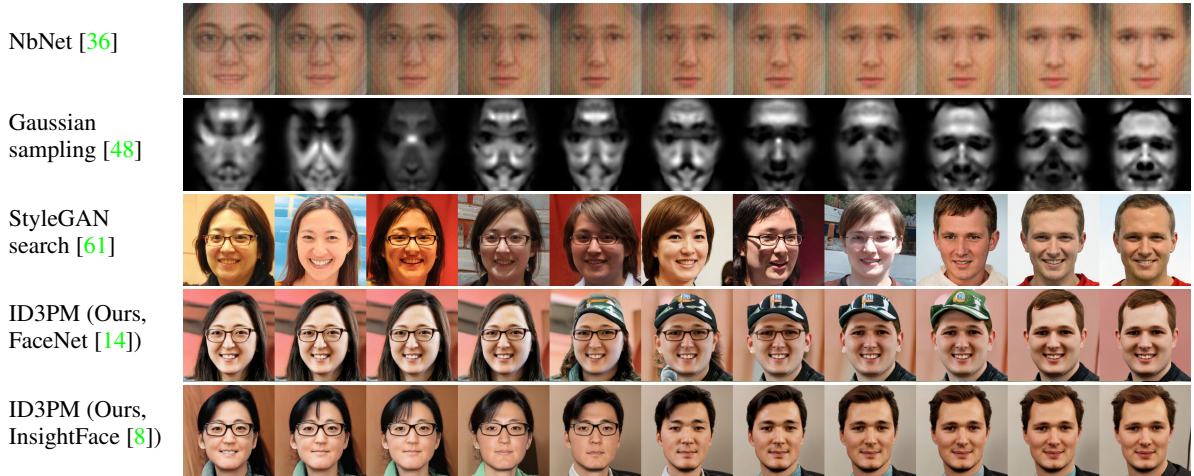
Table 7: Quantitative evaluation similar to Tab. 2 but with different values for the classifier-free guidance  $s$  for our models trained using ID vectors from FaceNet [14] and InsightFace [8]. The best performing setting for each ID vector is marked in bold.

<sup>3</sup>Note that we use the generated images of size  $64 \times 64$  (rather than the upsampled images) for computational reasons.

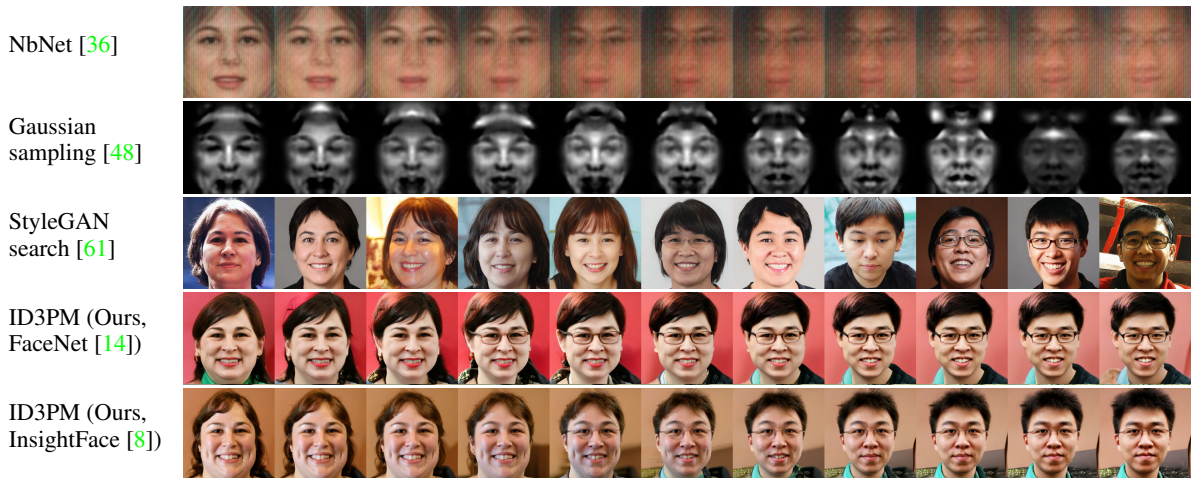


## C.2 Identity vector latent space

Our method is the first to our knowledge to enable smooth interpolations in the ID vector latent space. While we can condition other methods on an interpolated or adapted ID vector as well, their results lack realism and/or do not transition smoothly between images. This is demonstrated in the identity interpolations in Fig. 10. Note that spherical linear interpolation was used for all methods, but linear interpolation leads to a similar performance. The other one-to-many approaches, Gaussian sampling [48] and StyleGAN search [61], were extended such that the seed of all random number generators is set before each image is generated to eliminate discontinuities due to the randomness of the generation process. Nevertheless, certain non-identity characteristics, such as the expression, pose, and background for StyleGAN search [61], change from one image to the next.



(a) Identity 1  $\longleftrightarrow$  Identity 2



(b) Identity 3  $\longleftrightarrow$  Identity 4

Figure 10: Identity interpolations for two pairs of identities using state-of-the-art methods. Our method is the only method that provides realistic, smooth interpolations.

As described in Sec. 4.3, we can find custom directions in the ID vector latent space. This allows us to change certain identity-specific features such as the age, glasses, beard, gender, and baldness during image generation by traversing along a given direction as visualized in Fig. 11.

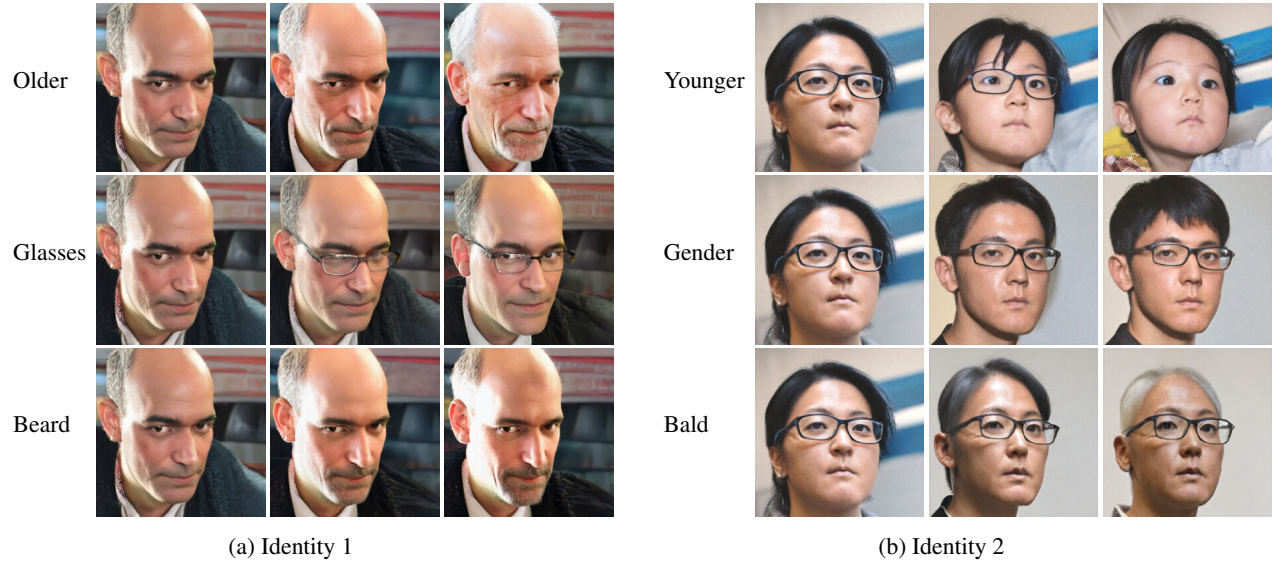


Figure 11: Controllable image generation through custom directions in the (InsightFace [8]) ID vector latent space.

### C.3 Attribute conditioning

To help disentangle identity from non-identity features as well as to obtain additional intuitive control, we propose attribute conditioning in Sec. 4.3. We thereby consider three sets of attributes from the FFHQ metadata [6]<sup>4</sup> as shown in Tab. 8 by grouping them by how much they contribute to a person’s identity. For example, set 1 (which was used in the main paper) only contains attributes that are identity-agnostic whereas set 3 also contains attributes that are strongly correlated with identity.

Attribute	Number of classes	Set		
		1	2	3
Age	1	✗	✗	✓
Emotion	8	✓	✓	✓
Facial hair	3	✗	✗	✓
Hair	8	✗	✗	✓
Head pose	3	✓	✓	✓
Gender *	1	✗	✗	✓
Glasses	1	✗	✓	✓
Makeup	2	✗	✓	✓
Occlusions	3	✗	✓	✓

Table 8: Different attribute sets. The number of (potentially identity-correlated) features increases from left to right.

\* While gender arguably falls on a continuous, nonlinear spectrum, we treat it as a binary variable since only this information is available in the data set.

By training our models with attribute conditioning, we can obtain images that recover more of the original data distribution when we sample conditioned on the identity but using the unconditional setting for the attributes (*i.e.* –1-vector for the attribute vector), as shown in Fig. 6.

However, the attributes can overpower the identity information if the attribute set contains attributes that are heavily correlated with the identity. This is visualized in Fig. 12 where we condition our model trained with InsightFace [8] ID vectors on the same ID vector but different attribute vectors, specifically the ones of the first 10 images of the FFHQ test set ( $\{69000, 69001, \dots, 69009\}$ ). As we cannot show images from the FFHQ [24] data set as mentioned in Sec. 6, we instead supply a table with their main attributes. For example, image 69000 is of a happy 27-year old woman with brown/black hair and makeup whose head is turned slightly to the left. For attribute set 1, only the pose and emotion is copied. For attribute set 2, the makeup is also copied. For attribute 3, the gender is also copied, thus leading to an image of a woman for identity 2. In general, as we add more attributes, the original identity is changed increasingly more. Since attribute set 2 and beyond can alter the identity significantly, we opt for attribute set 1 in most cases.

The overpowering of certain attributes over the identity can also be seen in the quantitative results of the diversity and identity distances in Tab. 3. Even when conditioning on attribute set 1 (only pose and emotion), the average identity distance increases despite the visual results appearing similar in terms of identity preservation. We hypothesize that this is because most face recognition vectors (inadvertently) encode the pose and expression (see Appendix E) and are less robust to extreme poses and expressions. Therefore, for the identity distance, it is better to reconstruct a face with a similar pose and expression as the original image. Nevertheless, we argue for the attribute conditioning (using attribute set 1) for most use cases because it leads to more diverse results and allows for an intuitive control over attributes.

<sup>4</sup>We ignore the following attributes from the metadata: smile because it correlates with emotion; and blur, exposure, and noise because we are not interested in them for the purposes of this experiment.



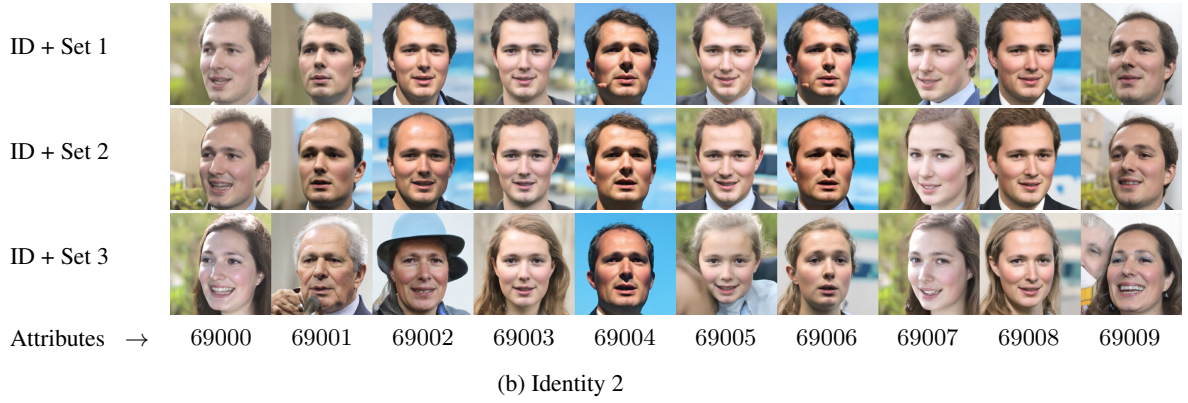
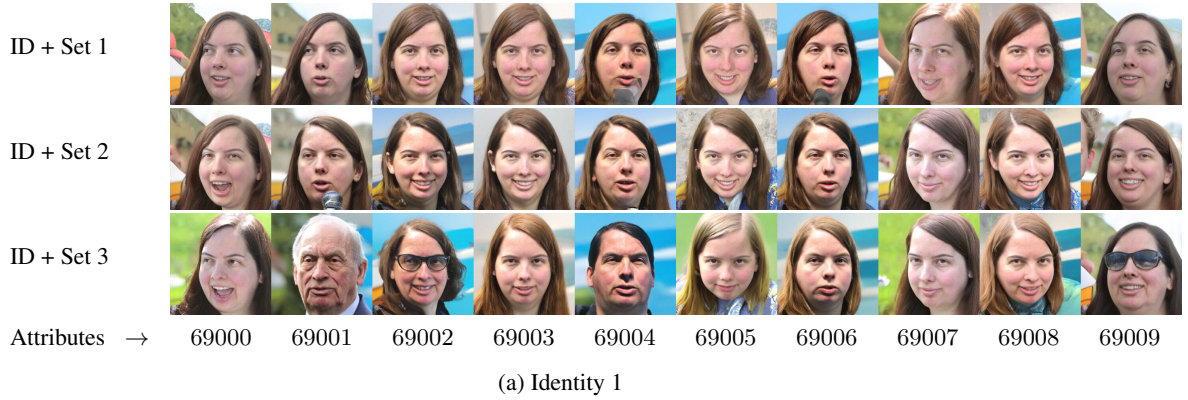


Image number	Gender	Age	Hair	Emotion	Yaw angle	Other
69000	Female	27	Brown/black	Happy	-21.9	Makeup
69001	Male	68	Gray	Neutral	-13.9	-
69002	Female	50	Not visible	Happy	5.5	Headwear + glasses
69003	Female	20	Brown/blond	Happy	-0.4	-
69004	Male	36	Black	Neutral	5.3	-
69005	Female	7	Blond	Happy	-2.6	-
69006	Female	18	Blond	Neutral	9.0	-
69007	Female	21	Brown	Happy	-24.3	Makeup
69008	Female	28	Blond	Happy	10.3	Makeup
69009	Female	43	Black/brown	Happy	-16.6	Makeup + glasses

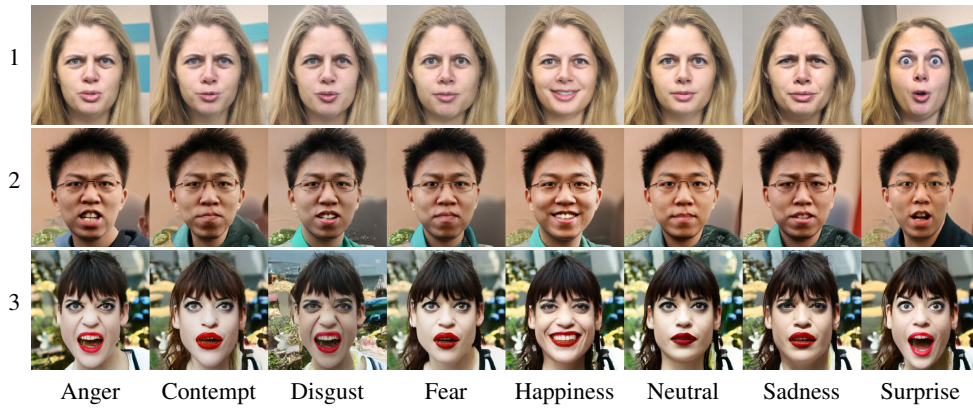
(c) Attribute descriptions

Figure 12: Attribute conditioning for two identities using different attribute sets. Images in each group have the same (InsightFace [8]) ID vector, but the attributes are chosen from images {69000, 69001, ..., 69009} of the FFHQ data set.

Through attribute conditioning, we can simply set the values of desired attributes, such as the emotion and head pose, during inference time to control them, as seen in Fig. 13. Note that our method has no internal structure to enforce 3D consistency. The attribute conditioning alone suffices in generating images that preserve the identity and 3D geometry surprisingly well as we traverse the attribute latent space. This intuitive attribute control paves the way towards using our method to create and augment data sets.



(a) Yaw angle



(b) Eight emotions

(c) Sad  $\longleftrightarrow$  Happy

Figure 13: Controllable image generation through attribute conditioning. We smoothly change three different attributes of three identities. All models were trained using InsightFace [8] ID vectors and attribute set 1.



## D Limitations

Our identity-preserving image generation method outputs images at a relatively low resolution of  $64 \times 64$ . While this can be upsampled using super-resolution models, some fine identity-specific details such as moles cannot be modeled currently (but this information might not even be stored in the ID vector). Our method also suffers from relatively long inference times (four minutes for a batch of 16 images and the super-resolution to  $256 \times 256$  on one NVIDIA RTX 3090 GPU) and small image generation artifacts, but this is expected to improve with future advancements in diffusion models.

Lastly, the diffusion model inherits the biases of both the face recognition model and the data set used to train the diffusion model. In addition to accessorizing images corresponding to certain demographic factors (*e.g.* via make-up, clothing), these biases cause our method to sometimes lose identity fidelity for certain underrepresented groups in the data sets. One such example is shown in Figure 14, where the method produces images quite different from the original identity.

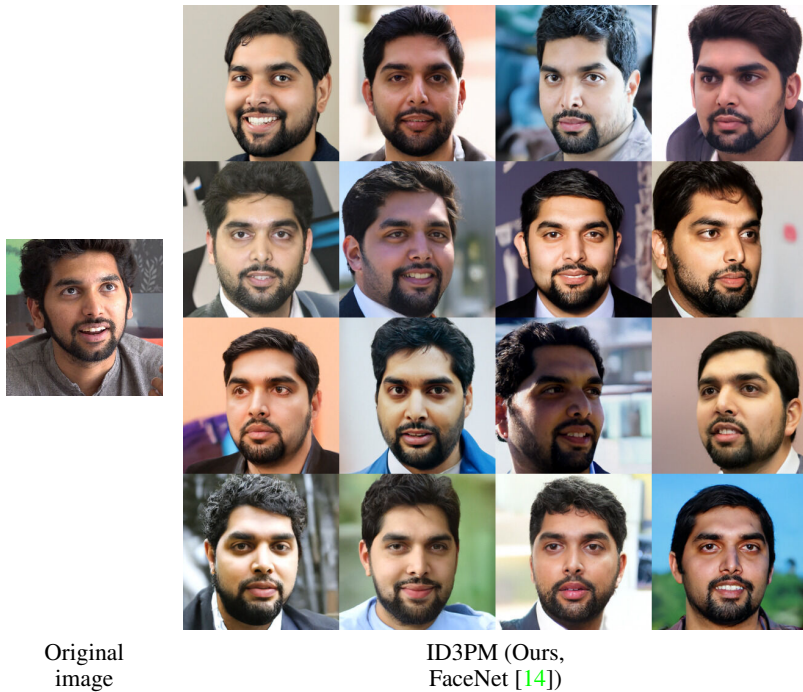


Figure 14: Failure case. Some underrepresented groups in the data sets might have lower identity fidelity for some ID vectors (here FaceNet [14]).

## E Application: Analysis of face recognition methods

With the rise of deep learning and large data sets with millions of images, face recognition methods have reached or even surpassed human-level performance [58, 57, 52, 44]. Nevertheless, face recognition systems have known issues in their robustness to different degradations and attacks [16, 55] and their biases (*e.g.* in terms of ethnic origin) [28, 59, 32].

Due to its general nature with very low requirements for the data set and few assumptions compared to other methods, our method is very well suited for analyzing and visualizing the latent spaces of different face recognition (FR) models. Since our method does not require access to the internals of the pre-trained face recognition model (*black-box* setting), we can analyze different face recognition methods by simply replacing the input ID vectors without worrying about different deep learning frameworks and the memory burden of adding more models.

For the analysis in this section, we train multiple versions of the model with ID vectors extracted with the pre-trained face recognition models listed in Tab. 4.

### E.1 Qualitative evaluation

Figure 15 shows uncurated samples of generated images of the considered ID vectors for several identities. While all generated images appear of a similar quality in terms of realism, the identity preservation of different methods behaves quite differently. The relative performance of different ID vectors changes depending on the identity, but the results for FaceNet [14] and InsightFace [8] seem most consistent on average<sup>5</sup>. As the inversion networks are trained with the same diffusion model architecture and the same data set, we hypothesize that these differences largely boil down to the biases of the respective face recognition methods and the data sets used to train them.

### E.2 Robustness

Our method can also be used to analyze and visualize the robustness of face recognition models in difficult scenarios such as varying expressions, poses, lighting, occlusions, and noise as seen in Fig. 16. In line with our previous observations, FaceNet [14] and InsightFace [8] appear the most robust.

In this analysis, it is also relatively easy to tell which features are extracted by observing which features of a target identity’s image are preserved. For example, ArcFace [10] and FROM [45] seem to contain pose information as the generated images in the fourth and fifth columns have a similar pose as the target identity’s image for both identities. Similarly, AdaFace [27] and ArcFace [10] seem to copy the expression for the third column of the first identity. InsightFace [8] also seems to contain expressions and pose for the second identity as seen in columns two to four. Another feature that is commonly copied is whether a person is wearing a hat or not even though this should arguably not be considered part of a person’s identity. Interestingly, FROM, a method specifically aimed to mask out corrupted features, does not appear more robust for the tested occlusions (sunglasses, hat). Lastly, noise seems to affect most face recognition methods significantly.

Figure 16 also lists the angular distances of the identities for each generated image to the target identity for the same FR method. The distances for generated images that can be considered failure cases are in general higher than those of the images that worked better. However, they are all still below the optimal threshold<sup>6</sup> calculated for each FR method for real images of the LFW [22] data set using the official protocol – meaning that all generated images are considered to be of the same person. Therefore, we argue that the wrong ID reconstructions are mostly due to problems in the ID vectors rather than the inversion of our model.

We further experiment with out-of-distribution samples such as drawings and digital renders as shown in Fig. 17. Interestingly, despite the extremely difficult setup, some of the resulting images resemble the identity fairly well, especially for FaceNet [14], demonstrating that some face recognition models can extract reasonable identity-relevant features even from faces that are out of distribution. Furthermore, this experiment shows that our method can generate extreme features, such as the large nose of the man in the fifth row with FaceNet [14], that are likely not in the training data set.

<sup>5</sup>Note that more images than the representative ones shown here were considered to make this statement and other statements in this section.

<sup>6</sup>It is actually the mean threshold over the 10 different splits. Note that the standard deviation across the splits is smaller than 0.005.

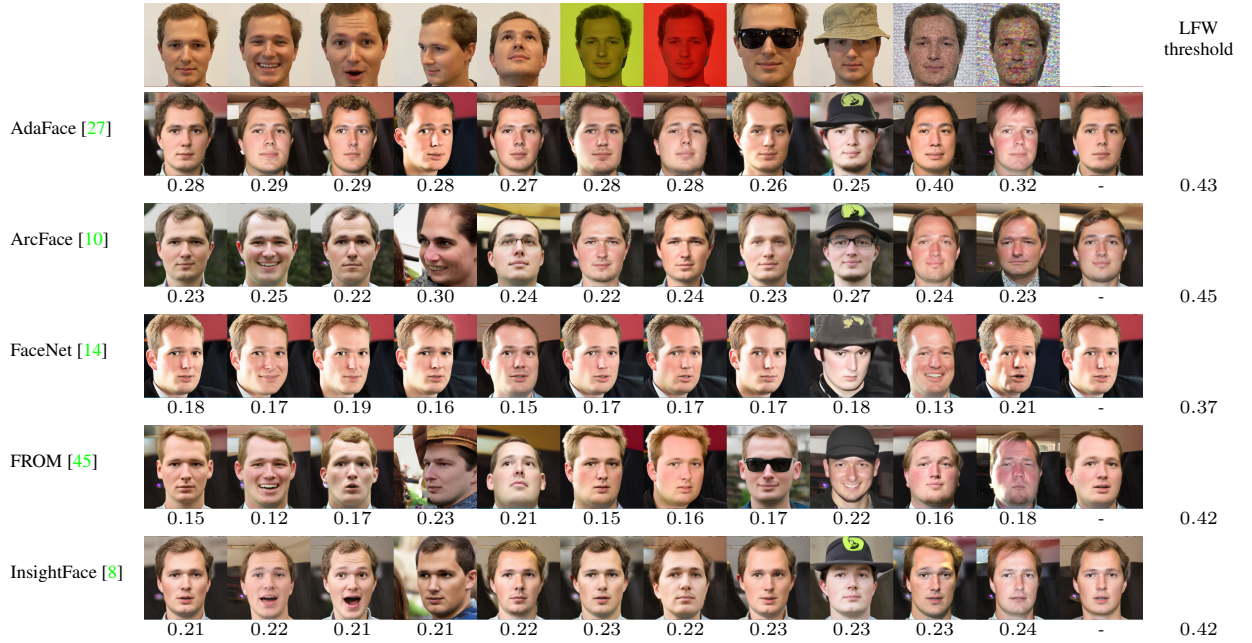




Figure 15: Qualitative evaluation of ID vectors from different state-of-the-art face recognition models. Note that the same seed was used for all images to obtain the most fair results.



(a) Identity 1



(b) Identity 2

Figure 16: Robustness experiment. The first row shows images of a source identity in challenging scenarios whereas the remaining rows show the results when using different ID vectors. The last image column shows images generated from the mean ID vector of all of the source identity images (for which no source image exists). The numbers under each line are the angular distances between the identity of the generated images and the target identity for the same face recognition method. The numbers in the last column are the optimal thresholds for that method calculated using real images of the LFW [22] data set and official protocol.



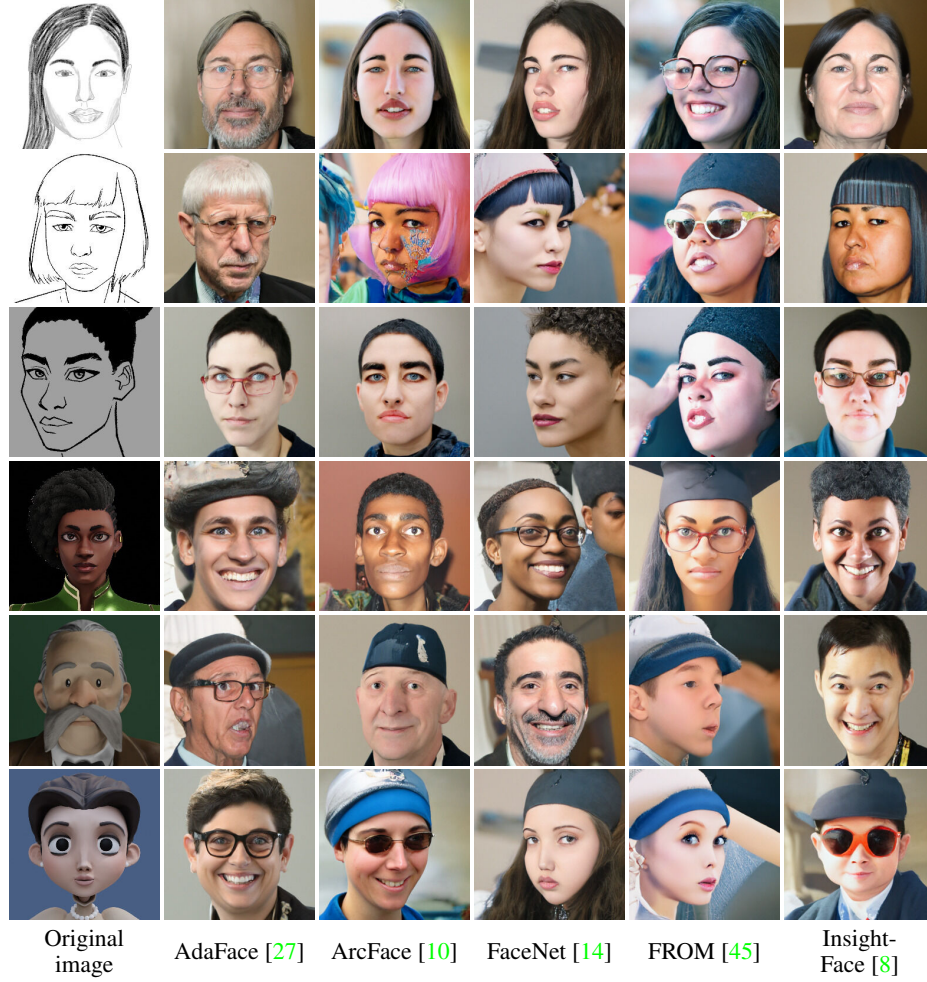


Figure 17: Robustness of ID vectors from different state-of-the-art face recognition models for out-of-distribution samples. Note that the same seed was used for all images to obtain the most fair results.

### E.3 Identity interpolations

By interpolating between two ID vectors, our method can produce new, intermediate identities, as shown in Fig. 1 and in Fig. 18. This empirically demonstrates that the latent spaces of most face recognition methods are fairly well-structured. Note that we use spherical linear interpolation because it produces slightly smoother results compared to linear interpolation.



(a) Identity 1  $\longleftrightarrow$  Identity 2



(b) Identity 3  $\longleftrightarrow$  Identity 4

Figure 18: Identity interpolations for two pairs of identities using different ID vectors.



#### E.4 Principal component analysis

To analyze the most prominent axes within the latent space, we perform principal component analysis (PCA) on the ID vectors of all 70000 images of the FFHQ data set for all considered face recognition models. As seen in Fig. 19, the first principal component appears to mainly encode a person’s age while the subsequent components are more entangled and thus less interpretable. Note that we normalize the size of the steps along the PCA directions by the  $L_2$  norm of the ID vectors to ensure a similar relative step size for the different ID vectors. Further note that large steps along any direction can cause the resulting latent vector to leave the distribution of plausible ID vectors and can cause artifacts, which is expected.



Figure 19: Visualization of the first three principal component analysis axes for two identities using different ID vectors.

Rather than traversing along PCA directions, Fig. 20 shows how the images change when projecting the ID vectors onto the first  $\{1, 2, 4, 8, 16, 32, 64, 128, 256, 512\}$  PCA axes. The main insight from this experiment is that the ID vectors from some face recognition models, such as FaceNet [14], can be compressed to as few as 64 dimensions without changing the perceived identity while others, such as AdaFace [27], require all 512 dimensions.

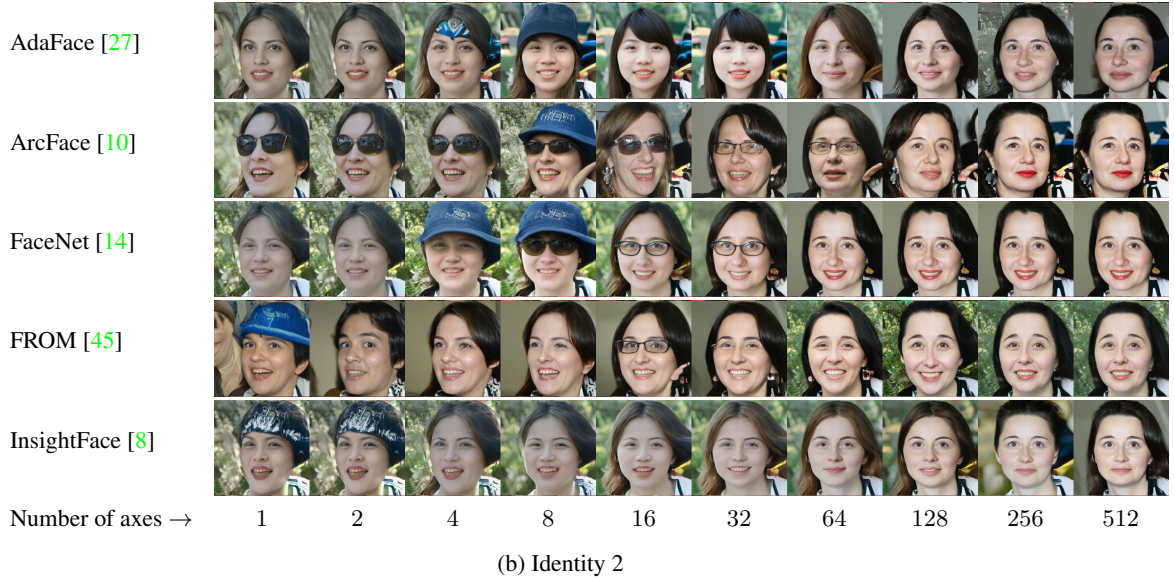
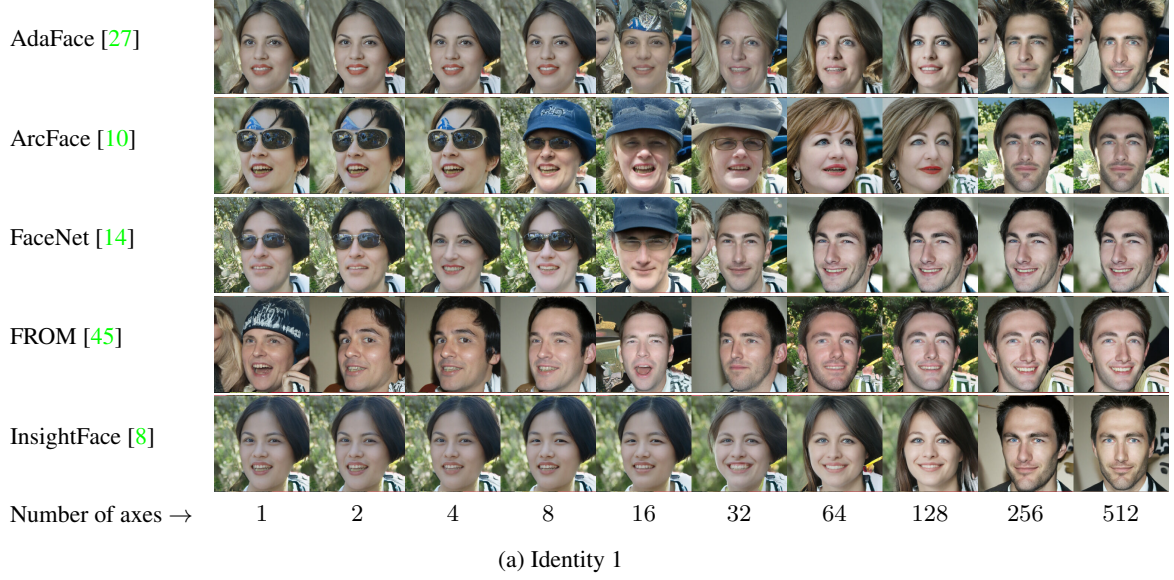


Figure 20: Visualization of the projections onto the first  $\{1, 2, 4, 8, 16, 32, 64, 128, 256, 512\}$  principal component analysis (PCA) axes for two identities using different ID vectors.



### E.5 Custom directions

Since the PCA axes are difficult to interpret, we calculate custom directions for each face recognition model as described in Sec. 4.3. As the biases of the FFHQ data set used to train our inversion models are the same for all ID vectors (*e.g.* glasses appearing when increasing the age direction), the presence or absence of certain directions in the latent space along which a given feature can be changed give insights about what information is extracted by a given face recognition model. As seen in Fig. 1 and Fig. 21, directions that are expected to be contained in the ID vector, such as the age and the gender, can be traversed smoothly. Furthermore, directions that may or may not be considered as part of the identity, such as the current look of a person (*e.g.* glasses, hair style, facial hair style), are also commonly contained as seen in the examples with the blond hair color in Fig. 21.



Figure 21: Visualization of custom direction modifications for two identities using different ID vectors for two directions that can be considered to belong to a person’s identity.

Most interestingly, our method reveals that some directions, such as the pose and emotion of a person, that arguably do not belong to a person’s identity can be found for some face recognition models as seen in Fig. 22. For example, ArcFace [10], FROM [45], and InsightFace [8] seem to (inadvertently) extract pose information as the yaw angle can be controlled somewhat by moving along the corresponding direction in the ID vector latent space. Similarly, the smile appears to be controllable in some small region for all considered ID vectors. Note that the goal of looking at these non-identity directions in the ID vector latent space is not necessarily to control this specific dimension cleanly (this can be achieved with attribute conditioning), but rather to analyze what information is extracted by a given FR method. Thus, our method can be used as a tool to reveal and visualize problems of FR methods that we might not even have been aware of and thus suggest hypotheses for further quantitative experiments.



Figure 22: Visualization of custom direction modifications for two identities using different ID vectors for two directions that arguably do not belong to a person’s identity. Our method reveals that many face recognition methods inadvertently extract non-identity information such as the pose and emotion.